

Factors driving entrainment in flotation systems and
implications for bank management

Nalini Singh

Supervisor: James A. Finch

Department of Mining and Materials Engineering
McGill University
Montreal, Quebec

A thesis submitted to McGill University in partial fulfilment
of a Masters in Engineering.

©Nalini Singh, 2013

December, 2013

Abstract

Entrainment is a non-selective form of flotation recovery which degrades the selectivity of the flotation process. Previous studies have found that a balanced recovery profile (i.e., each cell in a bank having equal recovery) yields the highest separation efficiency between two floatable minerals. Analysis of the empirical JKMRC water overflow rate model ($Q_w = aQ_s^b$) suggests that a balanced mass pull profile (i.e., equal mass distribution to each cell in bank) would minimise entrainment over a bank of flotation cells, whenever the value of b is greater than one.

Simulations conducted in JKSimFloat comparing varying recovery and mass pull profiles support a balanced mass pull profile to maximise the separation efficiency between a floatable mineral and entrained gangue, and a balanced recovery profile to maximise the separation efficiency between two floatable minerals.

Values of $b > 1$ were found for overflow rate data collected in several flotation systems. However, there was no phenomenological reasoning for this assumption. Based on data collected in industrial cells, the value of b was predicted in terms of the froth gas hold-up ($\epsilon_{g,f}$) and the fraction of unburst bubbles (α) that overflow a flotation cell ($b = \frac{\epsilon_{g,f}}{\alpha}$). The value of gas hold-up in flotation froths is typically greater than 50 %, whereas α is typically less than 50 %. This finding lends support to the assumption that b is always greater than 1. It is recommended that this model be tested on other systems to examine its validity.

Keywords: Flotation modelling, entrainment, bank management strategies

Résumé

L'entraînement est un mode non-sélective de flottation qui diminue la sélectivité du procédé de flottation. Des études précédentes démontrent qu'un profil de récupération balancée (dans laquelle chacune des cellules de flottation dans une série a une récupération équivalente) produit la meilleur efficacité de séparation entre deux minerais flottables. Une analyse du modèle empirique JKMRC du débit d'eau à la surverse ($Q_w = aQ_s^b$) suggère qu'un profil de récupération massique balancée (dans laquelle chacune des cellules de flottation dans une série a une récupération massique équivalente) minimiserait l'entraînement pour une série de cellules de flottation. Cette conclusion est valide seulement quand la valeur de b est supérieure à 1.

Des simulations comparant des profils de récupération et de récupération massique (réalisé avec le logiciel JKSimFloat) soutiennent qu'un profil de récupération massique balancée maximise l'efficacité de séparation entre un minerai flottable et des rejets non-flottables, et qu'un profil de récupération balancée maximise l'efficacité de séparation entre deux minerais flottables.

Des valeurs de $b > 1$ ont été mesurées pour des données de débits d'eau à la surverse dans plusieurs systèmes de flottation. Par contre, aucune explication phénoménologique n'existe pour justifier cette assumption. En utilisant des valeurs cueillies avec des cellules de flottation industrielles, la valeur de b a été prédit en terme de fraction gazeuse dans la mousse ($\epsilon_{g,f}$) et la fraction de bulles non-éclatées (α) dans la surverse de la cellule de flottation ($b = \frac{\epsilon_{g,f}}{\alpha}$). La valeur de la fraction gazeuse dans la mousse est généralement supérieur à 50 %, tandis que α est généralement inférieur à 50 %. Cette notion appui l'assumption que la valeur de b est toujours supérieur à 1. Il est recommandé que ce modèle soit vérifiée avec d'autres systèmes pour déterminer sa validité.

Mots-Clés: modélisation de systèmes de flottation, entraînement, gestion de série de cellules de flottation

Acknowledgements

It has truly been my honour and pleasure to ‘stand on the shoulders’ of the giant that is Professor Jim Finch. His enthusiasm and passion for knowledge and teaching have instilled in me a love of bubbles I didn’t know was possible. His advice and support have been crucial to the completion of my project and the main reason for which I may be able to ‘see further’.

I would like to thank the Minerals Processing group at McGill for their friendship, help, and support - in particular Ray Langlois for his invaluable assistance in the laboratory and crash courses in plumbing. It is truly with a heavy heart that I get ready to leave the group.

Financial support from NSERC, the Chair in Minerals Processing at McGill, and the Department of Mining and Materials Engineering are gratefully acknowledged. I am also grateful for the Department’s excellent administrative staff who have made navigating the non-academic side of McGill a breeze, and in particular, for her guidance and always open door: Barbara Hanley.

The assistance of Patrick Blonde in obtaining mineral samples and a fantastic opportunity to collect samples is gratefully acknowledged.

Lastly, but certainly not least, I would like to thank Sebastian Humphrey for being my moral support, sounding board, and chief remover of non-Oxford commas - your calm and unfailing logic have kept my stress levels at astoundingly low level during the compilation of my thesis.

Contents

1	Introduction	9
1.1	Flotation Models	10
1.2	The Need to Model Entrainment	11
1.3	Bank Organisation	12
1.4	Objectives, Scope, and Thesis Organisation	12
2	Literature Review	16
2.1	Froth Properties	16
2.1.1	Effect of Particles	17
2.1.2	Effect of Air Rate	17
2.2	Entrainment Models	18
2.2.1	Quantifying Entrainment	19
2.2.2	Empirical Models	20
2.2.3	Fundamental Models	23
2.2.4	Reagent Selection	25
2.3	Bank Management	26
2.3.1	Peak Air Recovery (PAR)	26
2.3.2	Air Profiling, and Mass Profiling	27
2.3.3	Recovery Profiling	27
2.4	Flotation Simulators	28
2.4.1	JKSimFloat	29
2.4.2	Integrated Geological Simulator (IGS)	30
3	Bank Profile Simulations	38
3.1	Modelling Entrainment	39
3.2	Simulator Set-up	41
3.2.1	Flotation Parameters	41
3.2.2	Simulation Methodology	43
3.3	Tested Profiles	45
3.4	The Two Floatable Mineral Case: Galena vs. Sphalerite	46

3.5	The Floatable Mineral vs. Entrained Mineral case: Galena vs. Gangue	48
3.6	Sensitivity Analysis	48
3.6.1	Effect of b	48
3.6.2	Use of Froth Recovery to Generate Profiles	49
3.6.3	Compositional Changes	50
3.6.4	Cell Size	51
3.7	Discussion	52
3.8	Conclusions	54
4	Experimental Apparatus and Procedures	56
4.1	Talc Properties	56
4.1.1	Degree of True Flotation	56
4.1.2	Composition and Size Distribution of Talc	58
4.1.3	Reagent Adsorption	59
4.2	Laboratory Overflow Tests	59
4.2.1	Denver Cell Experiments	60
4.2.2	Laboratory Column Experiments	60
4.2.3	Industrial Tests	63
5	Results	66
5.1	Denver Cell	66
5.2	Laboratory Column	69
5.3	Industrial Cells	70
6	Discussion	74
6.1	Alternative Water Overflow Rate Models	74
6.2	Froth Residence Time	77
7	Conclusions	83
A	Conversion of Recovery Basis	86
B	Raw Results	89
B.1	Experimental Check for the Miniature Column	89
B.2	Denver Cell DOE: Centre Point Repeats	90
C	Discussion Calculations	91

List of Figures

1.1	Schematic of a mechanical cell	10
1.2	Location of Particles in a Flotation System	12
2.1	Effect of particle size on the entrainment factor	18
2.2	Water recovery mechanisms from the pulp phase to the froth phase.	19
2.3	Schematic showing quantification of true flotation as per Warren (1985).	20
2.4	Simulated monodisperse foam showing bubbles, their lamellae, plateau borders and vertices. From Neethling et al. (2003).	24
2.5	Interaction between froth depth and air rate on the peak air recovery (PAR). From Hadler et al. (2012).	27
2.6	Schematic of a bank of cells. From Maldonado et al. (2011)	28
2.7	Breakdown of flotation feed into different classes. From Welsby (2009)	29
3.1	Solids and water overflow in a laboratory flotation column with 1 % solids	40
3.2	Screen shot of the JKSimFloat set-up used	42
3.3	Graphical representation of profiles tested in JKSimFloat	45
3.4	Galena-Sphalerite separation efficiency results for all simulations . .	47
3.5	Ratio of floatabilities between galena and sphalerite (S) down the bank	47
3.6	Galena-Gangue separation efficiency results for all simulations	48
3.7	Effect of increasing the value of b on the gain in separation efficiency between galena and gangue.	49
3.8	Variations in froth recovery with different ratios between mineral floatabilities	50
3.9	Difference in final grade between a balanced recovery and balanced mass pull profile showing the effect of varying feed composition. . . .	51
4.1	Ross test to measure the degree of true flotation for 15 % talc. . . .	57
4.2	Approximate composition of the talc used in laboratory scale experi- ments.	58

4.3	Laser particle size analysis before and after screening to remove some coarse material.	58
4.4	Fishbone diagram depicting factors affecting solids and water recovery from a flotation cell	59
4.5	Schematic of a Box Wilson design of experiment	60
4.6	Schematic of the set-up used for the laboratory column tests.	61
4.7	Schematic of the McGill Bubble Viewer used for sampling.	62
4.8	Sample bubble size image for processing in Northern Eclipse.	63
4.9	Schematic of the rougher bank on which samples were collected.	64
5.1	Results returned by DOEPro for the Denver experiment results shown in Table 5.1	68
5.2	Solids and water overflow rates for the Denver cell experimental results shown in Table 5.1	69
5.3	Overflow rates obtained using the miniature column system at increasing solids concentrations of talc.	70
5.4	Overflow rates in the roughing, cleaning, and scavenging banks.	71
5.5	Overflow rates in the roughing bank.	71
5.6	Overflow rates in the cleaning banks.	72
5.7	Sauter mean bubble size in the roughing bank.	72
6.1	Water overflow rates predicted by the Neethling et al. (2003) model compared to measured values.	76
6.2	Variation in overflow rate with froth velocity for the rougher bank.	77
6.3	Water overflow rates predicted by Equation 6.8 compared to measured values.	79
6.4	Overflow models defined by Equation 6.9 (Table 6.1) for each cell of the rougher bank.	79
6.5	Predicted water over flow rates (Equation 6.8) for the measured solids overflow rates.	80
6.6	Study of Gas hold up in flotation froths. From Tavera et al. (1998)	81
A.1	Schematic of a bank of cells. From Maldonado et al. (2011)	86
A.2	Balanced recovery based on cell feed shown with respect to both bank and cell feed.	87
B.1	Miniature column feed settings compared to the calculated feed.	89
B.2	Centre point repeats for the Denver cell design of experiment.	90

List of Tables

3.1	Feed Composition for Flotation Simulations	42
3.2	Mineral Floatabilities by Size–Used in Simulator Set-up	43
3.3	Gangue Entrainment Factors by Size Fraction.	43
3.4	Profiles evaluated using JKSimFloat.	45
3.5	Profiles evaluated using JKSimFloat, given in terms of bank feed. . .	46
3.6	Profiles evaluated using JKSimFloat, given as mass pull based on bank feed	46
4.1	Flotation reagents for bubble size control used in laboratory experi- ments.	59
4.2	Design of Experiment used to test the effect of solids concentration and air rate in a Denver cell	61
5.1	Overflow data for the first 30 seconds of Denver cell flotation.	67
5.2	Average bubble size and gas hold up data in the column	69
5.3	Measured Froth Velocities measured for the two air profiles tested. .	72
6.1	Values of a and b fitted by solver and tabulated using Equation 6.8 respectively	78
C.1	Rougher Bank Cell Parameters	91
C.2	Tabulated values of alpha.	92

Chapter 1

Introduction

Froth flotation can be considered the most important mineral separation technique of the past century. Since the original patent was filed in 1906, froth flotation has been expanded and applied to increasingly complex ores as well as greater tonnages (Wills and Napier-Munn 2006). The process exploits the physio-chemical properties of mineral surfaces to classify minerals. The necessary difference in surface chemistry between the minerals to be separated may be created/enhanced through the use of reagents (collectors, depressants, etc...) (Wills and Napier-Munn 2006).

In a flotation plant, mined ore is crushed, ground (often to less than 100 μm), and mixed with water to create a slurry. The slurry (which may be treated with reagents) is directed to a flotation machine (cell) where it is brought into contact with fine air bubbles, typically 0.5 to 2.5 mm in diameter. The mineral particles with hydrophobic surfaces attach to the air bubbles; the bubble-particle aggregate rises to the top of the machine to form a froth, which overflows to give the float product, which is commonly the valuable mineral (pay mineral) concentrate. This selective attachment to the bubble is termed true flotation (Smith and Warren 1989; Wills and Napier-Munn 2006) and these minerals will be referred to as 'floatable'. Minerals may also be non-selectively recovered by entrainment processes (Smith and Warren 1989; Wills and Napier-Munn 2006). Entrainment occurs when fine, low density particles are recovered due to the net upward flux of water in a flotation cell, the amount of entrainment being proportional to the amount of water recovered (Engelbrecht and Woodburn 1975).

The two types of recovery in a flotation cell, true flotation and entrainment, mean it is necessary to consider both the separation between two or more floatable minerals (all recovered by true flotation); and the separation between floatable and entrained minerals. It is the goal of a mineral processor to understand the system chemistry

in modulating true flotation, the system physics in modulating entrainment, and to use this information to obtain the highest economic recovery and grade of valuable mineral.

1.1 Flotation Models

The range of flotation reactions, sub-processes, and their interactions make it difficult to predict the final outcome of flotation, as it depends on the particular circumstances (chemical and physical conditions) (Ross 1998). A common view of flotation is to simplify it as a two-step process (Figure 1.1): mineral slurry is fed to the pulp zone where valuable mineral is collected and transported to the froth zone along with entrained particles. Some particles drop-back to the pulp zone from the froth zone due to drainage and detachment and may be collected again. Waste (gangue) mineral particles report to the non-float product stream (tailings). The concentrate is the valuable mineral plus any waste mineral that is transported through the froth zone. Three mechanisms have been identified which affect the transport of particles through the froth zone: drainage of water in the plateau borders (between bubbles), coalescence of bubbles, and sedimentation caused by the relative motion of particles and fluid (Johnson 2005; Cutting 1989). The interaction between the pulp and froth zone affects the overall performance of the flotation machine (Finch and Dobby 1990).

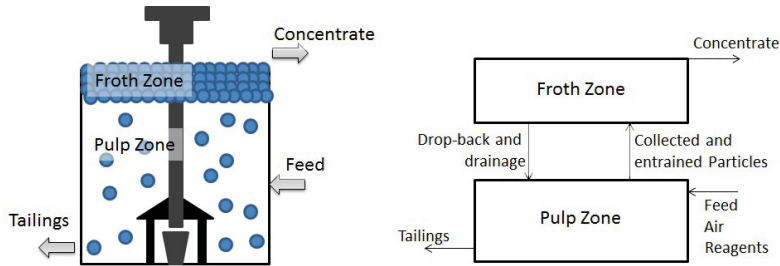


Figure 1.1: Schematic of a mechanical flotation cell and the simplified two-step process it represents. Modified from Subrahmanyam and Forsberg (1988).

The pulp zone of a flotation cell is assumed to be a well-mixed environment following first order kinetics such that the flotation recovery (R) can be related to a given rate constant (k) and the residence time of the system (τ) (Equation 1.1):

$$R = \frac{k\tau}{1 + k\tau} \quad (1.1)$$

The rate constant represents the intrinsic floatability of the material (P) as well as

machine factors, notably the bubble surface area flux, S_b . The overall rate constant for the cell (pulp and froth zones combined) is the rate constant of the pulp zone multiplied by froth recovery (R_f) (Equation 1.2) (Gorain et al. 1998):

$$K = PS_bR_f \quad (1.2)$$

This model does not account for entrainment: recovery due to entrainment (R_{ENT}) has been shown to be proportional to the amount of water recovered from the cell (R_w) (Equation 1.3) (Trahar 1981; Finch and Dobby 1990; Wills and Napier-Munn 2006). These components can be combined to give the overall recovery of a mineral (Equation 1.4) (Welsby 2009).

$$R_{ENT} = ENT \times R_w \quad (1.3)$$

$$R = \frac{PS_bR_f\tau(1 - R_w) + ENT R_w}{(1 + PS_bR_f\tau)(1 - R_w) + ENT R_w} \quad (1.4)$$

This model (Equation 1.4) is the one used by the Julius Krittchnitt Mineral Research Centre (JKMRC) to develop the JKSimFloat flotation simulator (Welsby 2009). There are other simulators (e.g., ModSim, IGS) which are also phenomenological in nature, combining physical and chemical principles with fitted parameters obtained from measured plant data (King 2001; SGS 2013).

1.2 The Need to Model Entrainment

Entrainment recovers particles indiscriminately from the flotation feed, degrading the selectivity of the process. It tends to affect fine, low density, particles preferentially as coarse particles are able to settle out of the water reporting to the concentrate. Particles in flotation exist in four different ways (Figure 1.2): in the pulp as a suspension, attached to bubbles in the pulp zone, attached to bubbles in the froth zone, and entrained in the plateau borders between bubbles (King 2001).

The need to model entrainment is evident as it is not possible to accurately predict grade without accounting for this major source of gangue recovery. Models of entrainment have relied on coupling entrainment with the water recovered from the cell (Smith and Warren 1989; Wills and Napier-Munn 2006). This implies that entrainment is implicit in the flotation process: without water it would not be possible for froth to overflow the cell. The degree of entrainment is dependent on a suite of variables including: froth depth, bubble size, air rate, particle size distribution,

reagent selection, the use of wash water, as well as the temperature of the pulp (Ross 1998).

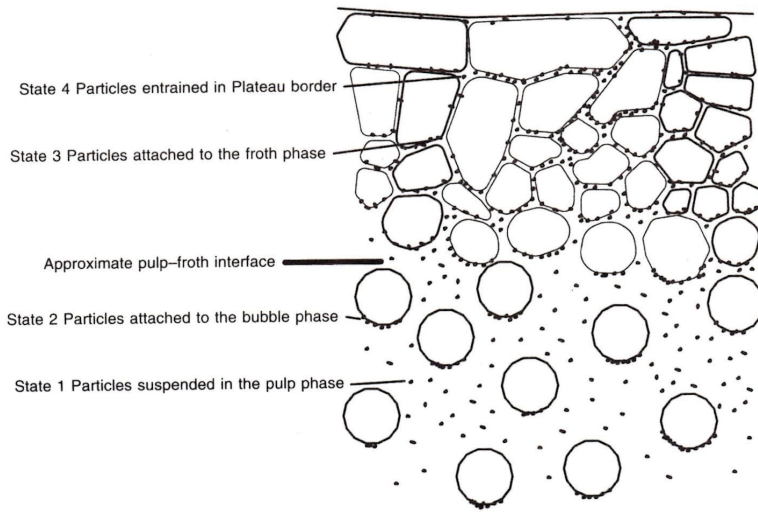


Figure 1.2: Location of Particles in a Flotation System. From King (2001).

1.3 Bank Organisation

In a plant, flotation cells are arranged in series into banks (or lines or rows). Using a bank of cells reduces the impact of mixing: well-mixed cells arranged into a bank approximate plug flow (Nesset 1988). The configuration of cells into banks poses an interesting question: is there a way to operate the bank to maximise performance? Gorain (2005) noted there is little rational basis for selecting an operating strategy for a bank of cells. Recently various research groups have examined this question (Cooper et al. 2004; Hadler and Cilliers 2009; Maldonado et al. 2011).

Of particular interest to this thesis is the modelling work of Maldonado et al. (2011; 2012) who found that for a bank of ‘ n ’ cells the best separation between two floatable minerals is given by a balanced (flat) recovery profile—i.e., the recovery in each cell should be equal (recovery being relative to the cell feed).

1.4 Objectives, Scope, and Thesis Organisation

The scope of this thesis is to combine flotation simulations and experimental data to extend the work of Maldonado et al. (2011). The simulations will examine both the separation between two floatable minerals and between floatable mineral and

entrained gangue. The experimental section will focus on water recovery models and their implications for entrainment minimisation.

Chapter 2: Literature review

The literature review will cover true flotation, entrainment, in particular the role of the froth and empirical and fundamental entrainment models. The experimental results will be considered in terms of these entrainment models in Chapter 6.

Chapter 3: Bank profile simulations

Flotation simulations conducted in JKSimFloat will be used to examine the effect of bank profile (i.e., the variation in recovery in cells down the bank) on the performance of the bank (with respect to floatable and entrained minerals). JKSimFloat was chosen as it is able to run many simulations at once.

Chapter 4: Experimental

The laboratory and plant experimental setups and conditions used to examine water and solids overflow in a talc system are described. Included are the descriptions and definitions of various hydrodynamic parameters collected during the experiments (gas hold-up, bubble size, superficial gas velocity).

Chapter 5: Results

The results are examined looking for relationships between solids and water overflow of a flotation cell.

Chapter 6: Discussion

The results of Chapter 5 will be discussed with regard to the entrainment models of Chapter 2.

Chapter 7: Conclusions

The conclusions of each chapter will be summarised with insights on bank management gained during simulations and analysis of experimental results.

Bibliography

- [1] M. Cooper, D. Scott, R. Dahlke, J.A. Finch, and C.O. Gomez. “Impact of air distribution profile on banks in a Zn cleaning circuit”. In: *CIM Bulletin* 97.1083 (2004), pp. 1–6.
- [2] G.W. Cutting. “Effect of Froth Structure and Mobility on Plant Performance”. In: *Mineral Processing and Extractive Metallurgy Review* 5 (1989), pp. 169–201.
- [3] J.A. Engelbrecht and E.T. Woodburn. “The effect of froth height, aeration rate and gas precipitation on flotation”. In: *Journal of South African Institute of Mining and Metallurgy* 10 (1975), pp. 125 –132.
- [4] J. A. Finch and G. S. Dobby. *Column flotation*. Oxford, England; New York: Pergamon, 1990.
- [5] B. K. Gorain, M. C. Harris, J. P. Franzidis, and E. V. Manlapig. “The effect of froth residence time on the kinetics of flotation”. In: *Minerals Engineering* 11.7 (1998), pp. 627–638.
- [6] B.K. Gorain. “Optimisation of flotation circuits with large flotation cells”. In: ed. by G.J. Jameson. Centenary of Flotation Symposium, AusIMM. Brisbane, Australia, 2005.
- [7] K. Hadler and J. J. Cilliers. “The relationship between the peak in air recovery and flotation bank performance”. In: *Minerals Engineering* 22.5 (2009), pp. 451–455.
- [8] N.W. Johnson. “A Review of the Entrainment Mechanism and its Modelling in Industrial Flotation Processes”. In: *Centenary of Flotation Symposium*. Ed. by Dr. Graeme Jameson. AusIMM, 2005, p. 487.
- [9] R.P. King. “Flotation”. In: *Modelling and Simulation of Mineral Processing Systems*. Butterworth-Heinemann, 2001. Chap. 9.
- [10] M. Maldonado, R. Araya, and J.A. Finch. “Optimizing flotation bank performance by recovery profiling”. In: *Minerals Engineering* 24.8 (2011), pp. 939–943.

- [11] M. Maldonado, R. Araya, and J.A. Finch. “An overview of optimising strategies for flotation banks”. In: *Minerals* 2 (2012), pp. 258–271.
- [12] J.E. Nasset. “The application of residence time distributions to flotation and mixing circuits”. In: *CIM Bulletin* (1988), pp. 75–83.
- [13] V.E. Ross. “Mechanisms operating in flotation froths”. In: *Frothing in Flotation II*. Ed. by J.S. Laskowski and E.T. Woodburn. Amsterdam: Gordon and Breach Science Publishers, 1998. Chap. 4.
- [14] SGS. *Integrated Geological Simulator*. 2013. URL: <http://www.sgs.com/en/Mining/Metallurgy-and-Process-Design/Geometallurgy/Predicting-Operational-Variables/IGS-Integrated-Geometallurgical-Simulator.aspx>.
- [15] P.G. Smith and L.J. Warren. “Entrainment of particles into flotation froths”. In: *Mineral Processing and Extractive Metallurgy Review* 5 (1989), p. 22.
- [16] T. V. Subrahmanyam and E. Forsberg. “Froth stability, particle entrainment and drainage in flotation A review”. In: *International Journal of Mineral Processing* 23.12 (1988), pp. 33–53.
- [17] W. J. Trahar. “A rational interpretation of the role of particle size in flotation”. In: *International Journal of Mineral Processing* 8.4 (1981), pp. 289–327.
- [18] S.D.D. Welsby. “On the interpretation of floatability using the bubble load”. PhD thesis. University of Queensland, 2009.
- [19] B. A. Wills and T. Napier-Munn. “Froth Flotation”. In: *Mineral Processing Technology*. Oxford: Butterworth-Heinemann, 2006, pp. 267–352.

Chapter 2

Literature Review

Froth flotation exploits the differences between hydrophobic and hydrophilic mineral surfaces to separate valuable minerals from each other and waste (gangue) minerals. Particles can be recovered via true flotation (bubble–particle attachment) or by entrainment (as a function of water recovery) (Wills and Napier-Munn 2006). Any flotation model must describe: bubble–particle collision, attachment, detachment, particle retention time in the froth and pulp, and hydraulic settling of particles (Ahmed and Jameson 1989; Ross 1998). This complexity poses a difficulty for fundamental modelling; flotation models are often empirical or semi–empirical in nature, relying on fitted parameters to represent a given system (King 2001).

As outlined in the introduction, froth flotation can be regarded as a two zone process: the pulp (collection) and froth zones (Figure 1.1). In a well–mixed cell, the effect of the froth zone on overall kinetics can be factored by the froth recovery ($K = PS_bR_f$). The froth properties constrain recovery from the collection zone, for both entrained and true floating particles.

This literature review will focus on: froth properties; empirical and fundamental models for entrainment and water recovery; existing rationales for bank management, to provide context for examining bank optimisation; and commercial flotation simulation software that is available.

2.1 Froth Properties

The froth zone can be considered the rate limiting step of the flotation process: particles collected in the pulp will not be recovered if they are not carried through the froth zone. There are a multitude of sub–processes occurring in the froth:

liquid and solids drainage, bubble coalescence, particle attachment/detachment, and entrainment—all affected by the size distribution and degree of hydrophobicity of the particles in the system (Ata 2012; Dippenaar 1982). A common froth metric is stability, which gives an indication of froth zone recovery. For example, a rigid, highly stable froth would inhibit drainage and promote entrainment (Zhang 2010). Some degree of stability is required to support the particle load of the froth. It is of interest to determine how froth properties may be altered to control grade and recovery, particularly with respect to measurable plant parameters. For example, a relationship between concentrate grade and froth velocity (measured using cameras) was used to improve metallurgical performance at the Northparkes concentrator (Rio Tinto) (Runge et al. 2007).

2.1.1 Effect of Particles

Froth stability is affected by frother composition and concentration; particle size, shape, hydrophobicity, and flocculation; and the presence of cations and other reagents (Finch et al. 2008; Kirjavainen 1996; Hunter et al. 2008). Maximum froth stability may be achieved using moderately hydrophobic particles (Ata 2012; Johansson and Pugh 1992) as highly hydrophobic particles (with some critical contact angle) tend to destabilise the froth by promoting coalescence (Hunter et al. 2008; Schwarz and Grano 2005).

The recovery of coarse particles by the froth is more sensitive to operating conditions whereas the froth poses less of a barrier to fine particle recovery (Rahman et al. 2012). Rahman et al. (2012) also observed that a certain amount of fine particles are required to ‘enhance’ coarse particle flotation. Zanin et al. (2009) found that the predominant factor affecting froth stability is the solids concentration in the pulp.

2.1.2 Effect of Air Rate

Barbian et al. (2003) found that air flow rate and frother concentration affected the dynamic foam stability factor (ratio of the volume of froth to air flow rate) and that this relationship could be used to predict the amount of air overflowing the weir when operating below the maximum equilibrium froth height.

Zheng et al. (2004b) determined that air residence time in the froth follows a plug flow model, independent of cell size if there is no bubble breakage on the surface of the froth—however it is readily observed that bubbles do burst (Zheng et al. 2004b; Ross 1998; Runge et al. 2007). The froth retention time can be modified by changing froth depth and air velocity as well as by changing cell dimensions by the presence

of a froth crowder (Zheng et al. 2004b). Zheng and Knopjes (2004) found that froth velocity varied linearly with air velocity, but not with froth height.

These studies highlight the importance of solids concentration, air velocity, frother type and dosage, and froth depth in controlling froth properties and therefore froth recovery due to true flotation as well as entrainment. As mentioned—a highly stable, rigid froth may restrict drainage of water increasing entrainment recovery, but some degree of froth stability is required to transport attached particles. The best froth properties for a cell depend on the system: the maximum froth stability may result in a high recovery, but not necessarily the best cell performance (Ata 2012).

2.2 Entrainment Models

Recovery due to entrainment is proportional to the amount of feed water recovered from the cell, with the degree of proportionality dependent on particle size (Figure 2.1). As particles increase in size, they are more likely to drain hydraulically: particles larger than $50 \mu m$ experience little to no entrainment (Johnson 2005). Feed water can be recovered in a bubble’s wake; in a thin layer of water surrounding each bubble; or from water drawn up by a bubble swarm (Johnson 2005; Warren 1985) (Figure 2.2).

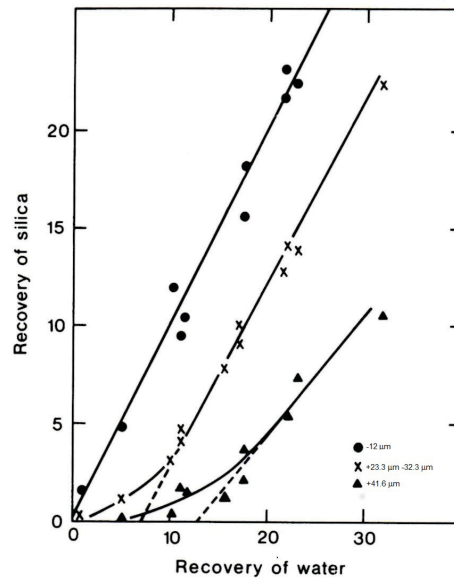


Figure 2.1: Effect of particle size on the recovery of silica due to entrainment showing that as size increases the entrainment factor decreases. From Engelbrecht and Woodburn (1975).

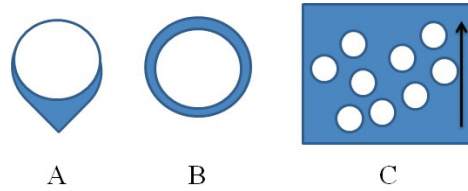


Figure 2.2: Water recovery mechanisms from the pulp phase to the froth phase: A- Bubble wake, B- Bound layer of bubble water, C- Water dragged upward by a bubble swarm.

Water can be removed from the froth by drainage, bubble coalescence and breakage, and sedimentation (Johnson 2005). There are numerous factors which affect the entrainment in a given system: air rate, bubble size, pulp chemistry, froth depth, gas hold-up in the pulp, particle size distribution, and slurry density (Valenta 2007; Wiese et al. 2011; Schwarz and Grano 2005). There have been a number of experiments performed to improve particle drainage and minimise entrainment: addition of wash water, vibrating the froth zone, and the use of reagents (e.g., high molecular weight polymers) to coagulate fines (Finch and Dobby 1990; Tao et al. 2000; Gong et al. 2010; Cao and Liu 2006).

Of particular interest to this thesis are entrainment models and the implications of these models for minimising entrainment. Due to the link between entrainment recovery and water recovery, models predicting entrainment often focus primarily on predicting the water recovery from the cell.

2.2.1 Quantifying Entrainment

Over the last three decades, several tests have been developed to quantify the degree of entrainment in a given system. Trahar and Warren (1976) proposed batch flotation experiments in the presence and absence of collector: particles recovered in the absence of a collector would be assumed to have been recovered by entrainment. This technique would be more relevant to coarse particles, as fines can be recovered at lower levels of hydrophobicity (George et al. 2004). Warren (1985) assumed that no entrainment could occur in a dry froth, such that on a plot of solids recovery against water recovery the intercept at zero water recovery would represent the recovery due to true flotation (Figure 2.3). Practically, this plot could be created by varying the froth height to alter water recovery (Warren 1985). Ross (1990) assumed that the percent solids of entrained particles in the froth and pulp are identical. This allows the mass of entrained material to be calculated from the mass of water recovered as the pulp percent solids are known. This model also assumes a constant froth depth - allowing for constant classification of material at the pulp froth interface (Ross

1990). A test was designed by George et al. (2004) utilising silica, alumina, and a cationic collector. The cationic collector would adsorb selectively onto silica but not onto alumina, therefore the recovery of alumina in the tests would be due to entrainment only (George et al. 2004). Cilek (2009) observed that the hydrophilic species in some complex ores are able to float due to self induced flotation, which may invalidate the results of the entrainment tests in some circumstances.

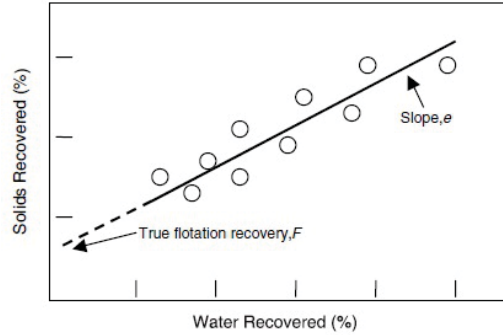


Figure 2.3: Schematic showing quantification of true flotation as per Warren (1985). From George et al. (2004).

2.2.2 Empirical Models

Models have been devised to predict entrainment from various systems (laboratory scale, pilot scale, and plant scale) encompassing a wide variety of modelling techniques including: neural networks, and linear and non-linear statistical models. Possibly the simplest model form is that developed by Alford (1990) and used in the JKSimFloat flotation simulator (Equation 2.1) which relies on two fitted parameters (a and b) to relate the solids overflow rate (Q_s) to the water overflow rate (Q_w) (Schwarz and Alexander 2006).

$$Q_w = aQ_s^b \quad (2.1)$$

In a series of papers Zheng et al. examined various aspects of the entrainment process. The first in the series examined the classification of particles at the pulp–froth interface (Zheng et al. 2004a). By collecting data from a variety of plant scale flotation machines a classification function (CF) was created to compare the partition between the mass of unattached particles in the pulp (ω_i^p) and tails (ω_i^t) (Equation 2.2). They found that the classification followed an exponential function with respect to particle size (d_p) (Equation 2.3) where λ and Φ are fitted constants. This finding re-confirms that predominantly fine particles are recovered by entrainment.

The study also found that cell size has a greater effect on the classification function than air rate and froth depth (Zheng et al. 2004a).

$$CF_i = \frac{\omega_i^p}{\omega_i^t} \quad (2.2)$$

$$CF_i = \Phi e^{-\lambda d_i} \quad (2.3)$$

Data were collected in a 3 m^3 Outokumpu cell to test against seven water recovery models: Alford (1990) (Equation 2.1); Uribe et al. (1999) (Equation 2.4); froth residence time (Savassi (1998) - Equation 2.5 and Gorain et al. (1998) - Equation 2.6); first order water recovery (Harris (2000) - Equation 2.7); drainage dominant model (Moys (1984) - Equation 2.8); and the fundamental model developed by Neethling and Cilliers (2002) (Equation 2.9). While the derivation is outside the scope of the thesis, the equations are presented as they appear in Zheng et al. (2006a) along with the parameters they utilise.

$$J_w = (aR_s^b + cJ_b)H_f^d D^e \quad (2.4)$$

where: a, b, c, d, and e are constants; J_w , the superficial water velocity; R_s , the solids recovery; J_b , the bias water velocity; H_f , the froth height; and D , the column diameter (original citation: Uribe et al. (1999)).

$$R_w = c\tau_f^d \quad (2.5)$$

where: c and d are constants; τ_f , the mean froth residence time (of air and solids); and R_w , the recovery of water (original citation: Savassi (1998)).

$$\frac{R_w}{1 - R_w} = \frac{R_{cw}}{1 - R_{cw}} e^{-\beta\tau_f} \quad (2.6)$$

where: R_{cw} is the recovery of water from the pulp phase to the froth phase; τ_f , the mean froth residence time (of air and solids); and β , a fitted constant (original citation: Gorain et al. (1998)).

$$R_w = 1 - \frac{1}{1 + P_w S_b \tau \Omega e^{(\sigma V_f - \chi \tau_f)}} \quad (2.7)$$

where: P_w is the rate constant for water recovery; S_b , the bubble surface area flux; τ ,

the residence time in the cell; ω, σ, χ , are constants; V_f , the volume of froth; and τ_f , the mean froth residence time (of air and solids) (original citation: Harris (2000)).

$$Q_w = AS_b\delta\alpha e^{-k_{wd}t_f} \quad (2.8)$$

where: A is the cross-sectional area; S_b , the bubble surface area flux; δ , the volume of water per surface area of the air bubbles; α , a factor that accounts for bursting bubbles; k_{wd} , the drainage rate constant of water; and t_f , the time it takes for the froth level to rise from the pulp interface to the launder (original citation: Moys (1984)).

$$Q_w = \alpha Q_a \frac{\epsilon_W}{1 - \epsilon_W} \quad (2.9)$$

where: α is the fraction of air bubbles that report, unburst, to the overflow; Q_a , the air flowrate in the froth zone; and ϵ_W , the water hold-at the top of the froth (original citation: Neethling and Cilliers (2003)).

Each of the seven models provided a good fit to the experimental data (the lowest R^2 reported was 0.84 for Equation 2.1) (Zheng et al. 2006a). However, Zheng et al. (2006a) pointed out that while all of the models involve fitted parameters, those of Alford (1990) and Uribe et al. (1999) do not include machine parameters. Ross (1998) noted that models are more valuable when they have predictive power. The model of Neethling and Cilliers (2002) was deemed superior as each variable has physical significance and as such would have greater predictive power.

Zheng et al. (2006b) next examined the relationship between water recovery and entrainment recovery. They observed that an increasing air rate increases entrainment recovery and an increasing froth depth causes a decrease entrainment recovery. This is consistent with the notion that increasing froth depth leads to increased drainage, whereas an increasing air rate drives more water up by increasing the bubble surface area flux. Under normal cell operating conditions, particles larger than $50 \mu m$ were not recovered by entrainment in this study (Zheng et al. 2006b).

A study of chromite entrainment in PGM processing found entrainment factors similar to those reported by Zheng et al. (2006b) (Hay and Roy 2010), with the majority of entrained particles in the $-38 \mu m$ fraction. Hay and Roy (2010) postulated that the recovery due to entrainment could be predicted by the total solids mass recovery in addition to the water recovery. Entrainment of fines was measured even in large flotation cells (Yianatos et al. 2009). The dependence of entrainment on particle size led Yianatos and Contreras (2010) to propose a model that includes both the

effect of grinding as well as froth stability (i.e., water recovery).

Cilek and Umucu (2001) employed a statistical design of experiment (DOE) approach to test the effect of various factors on gangue recovery: frother dosage, flotation time, air rate, froth depth, mass of fine and coarse particles, and percent solids. The experiments were carried out in a batch Denver cell, and they found a strong interaction between froth depth and air rate. In subsequent work Cilek and Ylmazer (2003), again using a DOE approach, examined the effect of air rate (V_a), percent solids (x), impeller speed, froth depth (T_f), and frother concentration on gangue recovery (R_g). They tried to interpret the results in terms of the Reynolds and Air Flow numbers, but were unable to obtain a satisfactory fit. Instead they performed neural network modelling to obtain Equation 2.10.

$$R_g = x^{0.2684} - 0.0276T_f(R_w^{-1.0311} - 0.1186V_a) \quad (2.10)$$

It is interesting to note that the gangue recovery in this model is proportional to the inverse of the water recovery (R_w), which is counter to the assumption of the water recovery models described in this section. However, they did not attempt to apply this recovery model to other systems.

2.2.3 Fundamental Models

In foam (i.e., with no solids present) bubbles are separated by water lamellae. These lamellae meet to form plateau borders (Figure 2.4) through which water can move (Neethling et al. 2000). A fundamental model of entrainment would need to account for the forces acting in the lamellae to describe the motion of water, such as capillary, gravitational, and viscous drag (Neethling et al. 2000). The forces are, in part, generated by pressure differences between the water and bubbles (Neethling et al. 2000). In a complete model, solids would also need to be considered: particles are either attached to the lamellae or are unattached i.e., particles dropped by coalescing or bursting bubbles or entrained particles (Neethling and Cilliers 2002; King 2001) (Figure 1.2). Unattached particles are able to move by hindered settling, geometric dispersion (the probability of a particle taking one path or another), or plateau border dispersion (particles in the centre of the border move faster than those near the edge) (Neethling et al. 2000).

The resulting model was complex, but Neethling et al. (2003) were able to simplify the relationships for a two phase foam (which is similar, but different to the model tested by Zheng et al. (2006a)). The model depends on the fraction of air (as unburst bubbles) that overflows the cell, α . The estimation of α depends on the froth velocity

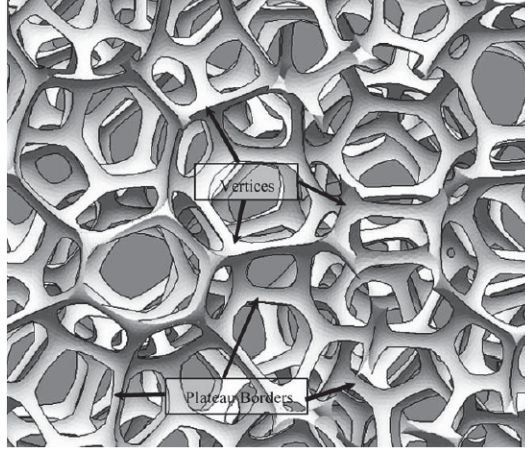


Figure 2.4: Simulated monodisperse foam showing bubbles, their lamallae, plateau borders and vertices. From Neethling et al. (2003).

overflowing the cell lip (v_{froth}), the height of froth above the lip (h_{lip}), the length of the cell lip (l_{lip}) and the volumetric air flow rate in the cell (Q_g). Two conditions exist depending on the value of α : $\alpha < 0.5$ and $\alpha > 0.5$ (Equation 2.11) (Neethling et al. 2003). If $\alpha < 0.5$, over half of the bubbles burst on top of the froth and the water overflow (Q_l) is described by Equation 2.12. If $\alpha > 0.5$, the overflow is described by Equation 2.13. The overflow is dependent on the cross-sectional area of the cell (A_{cell}), the gas velocity (v_g), the bubble size at the top of the froth (d_b) (through λ : $\lambda = \frac{1}{d_b^2}$), and k_l which represents the balance between the viscosity and density of the slurry. Note, the water overflow model does not depend on the froth height, the effect of froth height being captured by the impact on bubble size (the deeper the froth, the more coalescence and the larger the bubbles).

$$\alpha = \frac{v_{froth} h_{lip} l_{lip}}{Q_{air}} \quad (2.11)$$

$$Q_l = \frac{A_{column} v_g^2 \lambda}{k_l} (1 - \alpha) \alpha \quad (2.12)$$

$$Q_l = \frac{A_{column} v_g^2 \lambda}{4k_l} \quad (2.13)$$

When applying the model it is difficult to estimate the viscosity and density of the fluid in the plateau borders. In fact, as the amount of entrained material increases coalescence in the froth is reduced, likely due to an increase in the viscosity of lamellae fluid (Ata et al. 2003). The models developed by Neethling et al. (2000); Neethling and Cilliers (2002); Neethling et al. (2003) were used to create FrothSim,

which can be used to predict the effect of air rate changes in a plant (Smith et al. 2008).

Stevenson et al. (2003) points out that an assumption in the modelling of Neethling and Cilliers (2002) makes it valid only for dry froths. Stevenson et al. (2003) also raises the question of whether a high concentration of hydrophilic fines in the lamellae fluid may cause it to behave in a non-Newtonian way, changing the stresses in a mineralised froth. An alternate model was proposed by Stevenson (2007), which requires finding the solution to the differential equation presented as Equation 2.14.

$$\frac{\partial \epsilon}{\partial x} = \frac{p\rho g r_b \epsilon^{1-q}}{q\sigma} \left[\left(\frac{\epsilon j_g}{1-\epsilon} - j_{f*} + j_f \right) \frac{\mu}{\rho g r_b^2 m \epsilon^n} - 1 \right] \quad (2.14)$$

where: ϵ is the volumetric liquid fraction in the foam; x , the vertical dimension; p and q , are dimensionless numbers; ρ , the interstitial liquid density; g , the gravitational constant; r_b , the mean bubble radius; σ , the equilibrium surface tension; j_g , the superficial gas velocity; j_{f*} , the superficial liquid velocity to the overflow; j_f , the superficial liquid velocity; and μ , the interstitial liquid density.

2.2.4 Reagent Selection

For the model to be complete, flotation chemistry has to be included. While collector affects which particles will attach to bubbles, the role of frother is less intuitive. Frothers act to make small bubbles by preventing coalescence which both aids particle collection and stabilisation of the froth (Finch et al. 2008; Zhang 2009). Zhang (2009) measured the water overflow rate generated by various frothers in a two-phase system and found that frother type (chemistry) had a strong effect on the overflow rate that cannot be explained by differences in bubble size.

Different frothers produce different carrying rates of water into the overflow, apparently linearly proportional to the gas hold-up in the liquid below the froth (Moyo et al. 2007). This means that at a structural level frothers are able to influence the water recovery. This ability to influence water recovery is not necessarily the same in the presence and absence of solids (Melo and Laskowski 2006; Kuan and Finch 2010).

In addition to froth, it is possible to manipulate air dispersion properties using various salts (Craig et al. 1993; Pugh et al. 1997). While not all salts are able to inhibit coalescence, the ones that do are found to do so in proportion to the ionic strength of the solution (Quinn et al. 2007; Alexander et al. 2012). The effect of salts on coalescence may also influence water overflow rate.

2.3 Bank Management

Managing individual cells must be in the context of managing the bank of cells. The operating strategy of a bank must respect the operating range of the cells: e.g., the air rate must be high enough so that the cells do not sand out, but not so high as to boil (Dahlke et al. 2005). Apart from observing that operation will depend on the duty of the bank (e.g., roughing versus scavenging as discussed by Schwarz and Grano (2005)), Gorain (2005) noted there is little rational basis (strategy) for selecting individual cell operating conditions to optimise bank performance. This lack of strategy is particularly important dealing with entrainment in large cells where it is difficult to obtain good froth transport (Gorain 2005; Zhang 2009). Empirical and fundamental entrainment models can be used to find the factors that alter the entrainment behaviour. The models suggest that entrainment can be changed by altering the froth residence time, and the mass pull rate which can be achieved through the use of reagents, and machine parameters (Johnson 2005; Zheng et al. 2006a).

2.3.1 Peak Air Recovery (PAR)

Hadler and Cilliers (2009) suggested that the air rate needs to be linked with froth stability (as the latter is a driver of froth performance). Air recovery from the froth was used as a metric of froth stability (measured using video cameras) (Hadler and Cilliers 2009; Smith et al. 2010). Air is lost through bubbles bursting on the surface of the froth, and recovered when it reports as bubbles to the overflow launder. The air recovery was found to go through a maximum as the air rate was increased—this maximum was termed the peak air recovery (or PAR) (Hadler and Cilliers 2009; Smith et al. 2010) (Figure 2.5). Operating a bank of cells each at their PAR values provided greater cumulative pay mineral recovery at the end of the bank (Hadler and Cilliers 2009; Smith et al. 2010) attributed to improving froth stability and solids loading of the froth (Barbian et al. 2005).

Tests showed that PAR depends on froth depth (Hadler et al. 2012) (Figure 2.5). The best mineral recovery was obtained with a deep froth, even though a shallow froth depth gave a higher mass pull—this hints at a complex relationship between froth depth, air rate, and air recovery (Hadler et al. 2012).

PAR is expected to balance the needs of froth mobility and stability: at low air rates the froth is stable but immobile, allowing bubbles to burst before reaching the launder; conversely at high air rates, the froth is mobile but there are insufficient particles on the bubbles to stabilise the froth (leading to high coalescence) (Hadler

et al. 2012).

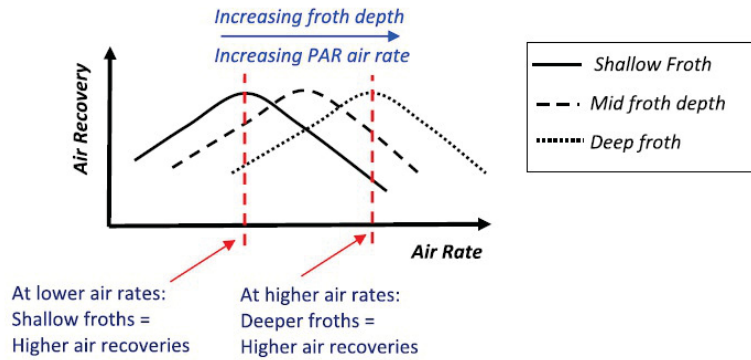


Figure 2.5: Interaction between froth depth and air rate on the peak air recovery (PAR). From Hadler et al. (2012).

2.3.2 Air Profiling, and Mass Profiling

In a trial at Xstrata’s Brunswick Mine the air to each cell was varied to create various air profiles (increasing, balanced, and decreasing) (Cooper et al. 2004). The increasing air profile gave the best grade–recovery curve. It was postulated that this occurred due to reduced entrainment down the bank, notably in the first cells in the bank, i.e., the ones with low air rates (Cooper et al. 2004). In this analysis it was observed that the ratio between the relative floatabilities of sphalerite and pyrite remained roughly constant down the bank (Cooper et al. 2004).

It was pointed out that in the air profiling studies the volume of air added to the bank was held constant and that there is no way of knowing whether that amount of air is optimal for the bank (Hadler et al. 2010). In testing the PAR concept Smith et al. (2010) tested four air profiles (as–found, stepped, sawtooth, and PAR) and found that PAR was able to give the best recovery and mass pull, however concentrate grade was sacrificed.

Runge et al. (2007) measured the froth velocity and collapse using froth cameras and used this to control the grade. In this way a froth velocity profile was considered to improve bank performance—a similar approach was also considered by Figueroa et al. (2009).

2.3.3 Recovery Profiling

Maldonado et al. (2011) conducted an analysis of the bank management question assuming first order kinetics and well–mixed individual cells (Equation 2.15). They

considered a two mineral system (A and B) with each mineral having a distinct floatability (k_A and k_B). Based on the findings of Cooper et al. (2004) it was assumed that the relative floatability between A and B was constant down the bank. The performance of the bank was judged by the separation efficiency (i.e., the recovery difference between the two minerals) at the end of the bank (Equation 2.16). Different profiles could then be compared for a given target recovery of mineral A (a higher separation efficiency implies a cleaner product). For a bank of n cells, Maldonado et al. (2011) were able to find a general solution: the recovery should be identical in each cell—relative to the feed to that cell (i.e., $R_{A1} = R_{A2} = \dots = R_{An}$) (Figure 2.6).

$$R_i = \frac{k_i \tau}{1 + k_i \tau} \quad (2.15)$$

$$S.E. = R_A - R_B \quad (2.16)$$

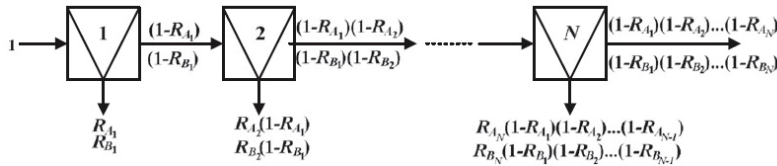


Figure 2.6: Schematic of a bank of cells. From Maldonado et al. (2011)

Maldonado et al. (2012) pointed out that at the heart of each profiling exercise is the underlying goal to control the recovery of a given mineral, while minimising the recovery of other minerals. They observed that air profiling and the PAR concept treat the problem in a local way (Maldonado et al. 2012).

2.4 Flotation Simulators

Several flotation simulation packages are available. The ModSim package was developed by King (2001) and offers the user three types of flotation model: King (1973), Sutherland (1989), and Klimpel (1980). The IGS simulator created by SGS (SGS 2013) emphasises concentrator modelling from grinding through to flotation. The JKSimFloat simulator is of particular interest to this thesis as it possesses a simulation manager which can be used to obtain various target recoveries from each cell to test various profiles (Schwarz and Alexander 2006).

The main difference between simulators is the way in which they treat the flotation rate constant as different particle sizes and types have different characteristics (Trahar 1981). For example, it is possible to consider the use of fast and slow floating components or the use of a distributed rate constant (Kelly and Carlson 1991). No one model has proved superior for each type of flotation bank; a rougher bank has a wider variety of particle types whereas feed to a cleaner bank has been preselected and should have a narrower distribution of particle types (Kelly and Carlson 1991).

2.4.1 JKSimFloat

JKSimFloat relies on the AMIRA P9 model introduced in Chapter 1 (Equation 2.17). Measured parameters are input to the software and the feed is lumped together by its properties (floatabilities, floatabilities by size, machine factors) (Figure 2.7). It is possible to choose multiple model components to complete the model, e.g., froth recovery can be specified as a fixed value, calculated by the froth residence time, or by using a drainage model (Schwarz and Alexander 2006).

$$R = \frac{PS_b R_f \tau (1 - R_w) + ENTR_w}{(1 + PS_b R_f \tau)(1 - R_w) + ENTR_w} \quad (2.17)$$

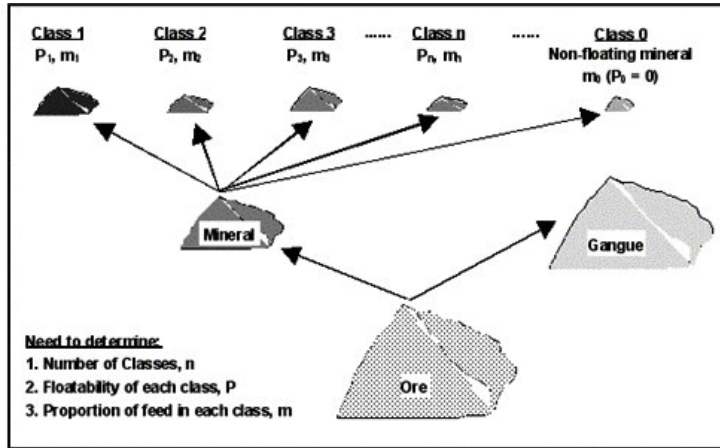


Figure 2.7: Breakdown of flotation feed into different classes. From Welsby (2009)

The machine factors (gas velocity, gas hold-up, froth recovery, cell volume, etc . . .) are specified at which point the software begins an iterative process: it assumes that 10% of the feed reports to the concentrate, after which the initial water recovery and residence time are calculated (Schwarz and Alexander 2006). Using the residence time and bubble surface area flux, the recovery of each particle class is calculated from the intrinsic floatability (P) of a mineral class. The process is repeated based on

the calculated recovery until the mass in each particle type converges (Schwarz and Alexander 2006). Simulations completed in JKSimFloat will be described in greater detail in Chapter 3 where it is used to test different recovery profile scenarios.

2.4.2 Integrated Geological Simulator (IGS)

The Integrated Geological Simulator developed by SGS aims to integrate simulations of processing plants starting from the crushing and grinding stages, thus incorporating a geometallurgical approach to modelling (SGS 2013). The final model form used in IGS is similar to that used in JKSimFloat, however the tabulation of the individual model constituents are different. For example, the water recovery from a cell can be specified as a fixed water flow per cell, or by fixing the solids density of the concentrate (SGS 2013). The rate constant specified in the software is used in the recovery calculation along with the residence time, however the machine parameters are lumped together as a froth recovery parameter.

Bibliography

- [1] N. Ahmed and G.J. Jameson. “Flotation Kinetics”. In: *Mineral Processing and Extractive Metallurgy Review* 5 (1989), p. 22.
- [2] S. Alexander, J. Quinn, J.E. van der Spuy, and J.A. Finch. “Correlation of Graphite Flotation and Gas Holdup in Saline Solutions”. In: *SME Annual Meeting: Water in Mineral Processing* (2012).
- [3] R.A. Alford. “An improved model for design of industrial column flotation circuits in sulphide applications”. In: *Sulphide Deposits - Their Origin and Processing*. Ed. by P.M.J. Gary. IMM London, 1990.
- [4] S. Ata. “Phenomena in the froth phase of flotation A review”. In: *International Journal of Mineral Processing* 102103.0 (2012), pp. 1–12.
- [5] S. Ata, N. Ahmed, and G.J. Jameson. “A study of bubble coalescence in flotation froths”. In: *International Journal of Mineral Processing* 72.14 (2003), pp. 255–266.
- [6] N. Barbian, E. Ventura-Medina, and J. J. Cilliers. “Dynamic froth stability in froth flotation”. In: *Minerals Engineering* 16.11 (2003), pp. 1111–1116.
- [7] N. Barbian, K. Hadler, E. Ventura-Medina, and J.J. Cilliers. “The froth stability column: linking froth stability and flotation performance”. In: *Minerals Engineering* 18 (2005), pp. 317–324.
- [8] Mingli Cao and Qi Liu. “Reexamining the functions of zinc sulfate as a selective depressant in differential sulfide flotation: The role of coagulation”. In: *Journal of Colloid and Interface Science* 301.2 (2006), pp. 523–531.
- [9] E. C. Cilek and Y. Umucu. “A statistical model for gangue entrainment into froths in flotation of sulphide ores”. In: *Minerals Engineering* 14.9 (2001), pp. 1055–1066.
- [10] E. C. Cilek and B. Z. Ylmazer. “Effects of hydrodynamic parameters on entrainment and flotation performance”. In: *Minerals Engineering* 16.8 (2003), pp. 745–756.

- [11] E.C. Cilek. “The effect of hydrodynamic conditions on true flotation and entrainment in flotation of a complex sulphide ore”. In: *International Journal of Mineral Processing* 90.14 (2009), pp. 35–44.
- [12] M. Cooper, D. Scott, R. Dahlke, J.A. Finch, and C.O. Gomez. “Impact of air distribution profile on banks in a Zn cleaning circuit”. In: *CIM Bulletin* 97.1083 (2004), pp. 1–6.
- [13] Vincent S. J. Craig, Barry W. Ninham, and Richard M. Pashley. “The effect of electrolytes on bubble coalescence in water”. In: *The Journal of Physical Chemistry* 97.39 (1993), pp. 10192–10197.
- [14] R. Dahlke, C. Gomez, and J. A. Finch. “Operating range of a flotation cell determined from gas holdup vs. gas rate”. In: *Minerals Engineering* 18.9 (2005), pp. 977–980.
- [15] A. Dippenaar. “The destabilization of froth by solids. II. The rate-determining step”. In: *International Journal of Mineral Processing* 9.1 (1982), pp. 15–22.
- [16] J.A. Engelbrecht and E.T. Woodburn. “The effect of froth height, aeration rate and gas precipitation on flotation”. In: *Journal of South African Institute of Mining and Metallurgy* 10 (1975), pp. 125 –132.
- [17] *Determination of rougher froth velocity profiles and their implementation through expert systems*. Proceedings of the VI International Mineral Processing Seminar (Procemin). Santiago, Chile, 2009.
- [18] J. A. Finch and G. S. Dobby. *Column flotation*. Oxford, England; New York: Pergamon, 1990.
- [19] J.A. Finch, J.E. Nasset, and C. Acua. “Role of frother on bubble production and behaviour in flotation”. In: *Minerals Engineering* 21.1214 (2008), pp. 949–957.
- [20] P. George, A. V. Nguyen, and G. J. Jameson. “Assessment of true flotation and entrainment in the flotation of submicron particles by fine bubbles”. In: *Minerals Engineering* 17.78 (2004), pp. 847–853.
- [21] J. Gong, Y. Peng, A. Bouajila, M. Ourriban, A. Yeung, and Qi Liu. “Reducing quartz gangue entrainment in sulphide ore flotation by high molecular weight polyethylene oxide”. In: *International Journal of Mineral Processing* 97.14 (2010), pp. 44–51.
- [22] B.K. Gorain. “Optimisation of flotation circuits with large flotation cells”. In: ed. by G.J. Jameson. Centenary of Flotation Symposium, AusIMM. Brisbane, Australia, 2005.

- [23] B.K. Gorain, M.C. Harris, J.-P. Franzidis, and E.V. Manlapig. “The effect of froth residence time of the kinetics of flotation”. In: *Minerals Engineering* 11 (1998), pp. 627–638.
- [24] K. Hadler and J. J. Cilliers. “The relationship between the peak in air recovery and flotation bank performance”. In: *Minerals Engineering* 22.5 (2009), pp. 451–455.
- [25] K. Hadler, C. D. Smith, and J. J. Cilliers. “Recovery vs. mass pull: The link to air recovery”. In: *Minerals Engineering* 23.1113 (2010), pp. 994–1002.
- [26] K. Hadler, M. Greyling, N. Plint, and J.J. Cilliers. “The effect of froth depth on air recovery and flotation performance”. In: *Minerals Engineering* 36-38 (2012), pp. 248–253.
- [27] T.A. Harris. “The development of a flotation simulation methodology towards an optimisation study of UG2 platinum flotation circuits”. PhD thesis. University of Cape Town, 2000.
- [28] M.P. Hay and R. Roy. “A case study of optimising UG2 flotation performance. Part 1: Bench, pilot and plant scale factors which influence Cr₂O₃ entrainment in UG2 flotation”. In: *Minerals Engineering* 23.1113 (2010), pp. 855–867.
- [29] T.N. Hunter, R.J. Pugh, G.V. Franks, and G.J. Jameson. “The role of particles in stabilising foams and emulsions”. In: *Advances in Colloid and Interface Science* 137.2 (2008), pp. 57–81.
- [30] G. Johansson and R. J. Pugh. “The influence of particle size and hydrophobicity on the stability of mineralized froths”. In: *International Journal of Mineral Processing* 34.12 (1992), pp. 1–21.
- [31] N.W. Johnson. “A review of the entrainment mechanism and its modelling in industrial flotation processes”. In: 2005, pp. 487–496.
- [32] E. G. Kelly and C. E. Carlson. “Two flotation models: Resolution of a conflict”. In: *Minerals Engineering* 4.12 (1991), pp. 1333–1338.
- [33] R.P. King. “Model for the design and control of flotation plants”. In: *Applications of Computer Methods in the Mineral Industry*. Ed. by M.D.G. Salmon and F.H. Lancaster. South African Institute of Mining and Metallurgy - Johannesburg, 1973, pp. 341–350.
- [34] R.P. King. “Flotation”. In: *Modelling and Simulation of Mineral Processing Systems*. Butterworth-Heinemann, 2001. Chap. 9.
- [35] V. M. Kirjavainen. “Review and analysis of factors controlling the mechanical flotation of gangue minerals”. In: *International Journal of Mineral Processing* 46.12 (1996), pp. 21–34.

- [36] R.R. Klimpel. “Selection of chemical reagents for flotation”. In: *Mineral Processing Plant Design, 2nd edition*. Ed. by A. Mular and R. Bhappu. SME, Colorado, 1980, pp. 907–934.
- [37] S.H. Kuan and J.A. Finch. “Impact of talc on pulp and froth properties in F150 and 1-pentanol frother systems”. In: *Minerals Engineering* 23.1113 (2010), pp. 1003–1009.
- [38] M. Maldonado, R. Araya, and J.A. Finch. “Optimizing flotation bank performance by recovery profiling”. In: *Minerals Engineering* 24.8 (2011), pp. 939–943.
- [39] M. Maldonado, R. Araya, and J.A. Finch. “An overview of optimising strategies for flotation banks”. In: *Minerals* 2 (2012), pp. 258–271.
- [40] F. Melo and J. S. Laskowski. “Fundamental properties of flotation frothers and their effect on flotation”. In: *Minerals Engineering* 19.68 (2006), pp. 766–773.
- [41] P. Moyo, C. O. Gomez, and J. A. Finch. “Characterizing Frothers using Water Carrying Rate”. In: *Canadian Metallurgical Quarterly* 46.3 (2007), pp. 215–220.
- [42] M.H. Moys. “Residence time distribution and mass transport in the froth phase of the flotation process”. In: *International Journal of Mineral Processing* 13 (1984), pp. 117–142.
- [43] S. J. Neethling and J. J. Cilliers. “The entrainment of gangue into a flotation froth”. In: *International Journal of Mineral Processing* 64.23 (2002), pp. 123–134.
- [44] S. J. Neethling and J. J. Cilliers. “Modelling flotation froths”. In: *International Journal of Mineral Processing* 72 (2003), pp. 267–287.
- [45] S. J. Neethling, J. J. Cilliers, and E. T. Woodburn. “Prediction of the water distribution in a flowing foam”. In: *Chemical Engineering Science* 55.19 (2000), pp. 4021–4028.
- [46] S. J. Neethling, H. T. Lee, and J. J. Cilliers. “Simple relationships for predicting the recovery of liquid from flowing foams and froths”. In: *Minerals Engineering* 16.11 (2003), pp. 1123–1130.
- [47] R. J. Pugh, P. Weissenborn, and O. Paulson. “Flotation in inorganic electrolytes; the relationship between recover of hydrophobic particles, surface tension, bubble coalescence and gas solubility”. In: *International Journal of Mineral Processing* 51.1-4 (1997), pp. 125–138.
- [48] J. J. Quinn, W. Kracht, C. O. Gomez, C. Gagnon, and J. A. Finch. “Comparing the effect of salts and frother (MIBC) on gas dispersion and froth properties”. In: *Minerals Engineering* 20.14 (2007), pp. 1296–1302.

- [49] R.M.. Rahman, S. Ata, and G. J. Jameson. “The effect of flotation variables on the recovery of different particle size fractions in the froth and the pulp”. In: *International Journal of Mineral Processing* 106109.0 (2012), pp. 70–77.
- [50] V. E. Ross. “Flotation and entrainment of particles during batch flotation tests”. In: *Minerals Engineering* 3.34 (1990), pp. 245–256.
- [51] V.E. Ross. “Mechanisms operating in flotation froths”. In: *Frothing in Flotation II*. Ed. by J.S. Laskowski and E.T. Woodburn. Amsterdam: Gordon and Breech Science Publishers, 1998. Chap. 4.
- [52] K. Runge, J. McMaster, M. Wortley, D. La Rosa, and O. Gu. “A correlation between Visiofroth measurements and the performance of a flotation cell”. In: *Ninth Mill Operators’ Conference*. AusIMM, 2007.
- [53] O.N. Savassi. “Direct estimation of the degree of entrainment and the froth recovery of attached particles in industrial flotation cells”. PhD thesis. University of Cape Town, 1998.
- [54] S. Schwarz and D. Alexander. *JKSimFloat V.6.1 PLUS: Improving flotation circuit performance by simulation*. 2006. URL: <http://www.jktech.com.au/sites/default/files/brochures/JKSimFloatMPMSC.pdf>.
- [55] S. Schwarz and S. Grano. “Effect of particle hydrophobicity on particle and water transport across a flotation froth”. In: *Colloids and Surfaces A: Physicochemical and Engineering Aspects* 256.23 (2005), pp. 157–164.
- [56] SGS. *Integrated Geological Simulator*. 2013. URL: <http://www.sgs.com/en/Mining/Metallurgy-and-Process-Design/Geometallurgy/Predicting-Operational-Variables/IGS-Integrated-Geometallurgical-Simulator.aspx>.
- [57] C. Smith, S. Neethling, and J. J. Cilliers. “Air-rate profile optimisation: From simulation to bank improvement”. In: *Minerals Engineering* 21.1214 (2008), pp. 973–981.
- [58] C. D. Smith, K. Hadler, and J. J. Cilliers. “Flotation bank air addition and distribution for optimal performance”. In: *Minerals Engineering* 23.1113 (2010), pp. 1023–1029.
- [59] P. Stevenson. “Hydrodynamic theory of rising foam”. In: *Minerals Engineering* 20.3 (2007), pp. 282–289.
- [60] P. Stevenson, C. Stevanov, and G. J. Jameson. “Liquid overflow from a column of rising aqueous froth”. In: *Minerals Engineering* 16.11 (2003), pp. 1045–1053.
- [61] D. N. Sutherland. “Batch flotation behaviour of composite particles”. In: *Minerals Engineering* 2.3 (1989), pp. 351–367.

- [62] D. Tao, G. H. Luttrell, and R. H. Yoon. “A parametric study of froth stability and its effect on column flotation of fine particles”. In: *International Journal of Mineral Processing* 59.1 (2000), pp. 25–43.
- [63] W. J. Trahar. “A rational interpretation of the role of particle size in flotation”. In: *International Journal of Mineral Processing* 8.4 (1981), pp. 289–327.
- [64] W.J. Trahar and L.J. Warren. “The floatability of very fine particles - a review”. In: *International Journal of Mineral Processing* 14 (1976), pp. 33 – 44.
- [65] A.S. Uribe, D.V. Vazquez, R.G. Perez, and F.A. Nava. “A statistical model for the concentrate water in flotation columns”. In: *Minerals Engineering* 12.8 (1999), pp. 937 –948.
- [66] M.M. Valenta. “Balancing the reagent suite to optimise grade and recovery”. In: *Minerals Engineering* 20.10 (2007), pp. 979–985.
- [67] L.J. Warren. “Determination of the contributions of true flotation and entrainment in batch flotation tests”. In: *International Journal of Mineral Processing* 14.1 (1985), pp. 33–44.
- [68] S.D.D. Welsby. “On the interpretation of floatability using the bubble load”. PhD thesis. Univeristy of Queensland, 2009.
- [69] J. Wiese, P. Harris, and D. Bradshaw. “The effect of the reagent suite on froth stability in laboratory scale batch flotation tests”. In: *Minerals Engineering* 24.9 (2011), pp. 995–1003.
- [70] B. A. Wills and T. Napier-Munn. “Froth Flotation”. In: *Mineral Processing Technology*. Oxford: Butterworth-Heinemann, 2006, pp. 267–352.
- [71] J. Yianatos and F. Contreras. “Particle entrainment model for industrial flotation cells”. In: *Powder Technology* 197.3 (2010), pp. 260–267.
- [72] J. Yianatos, C. Carrasco, L. Bergh, L. Vinnett, and C. Torres. “Modelling and simulation of rougher flotation circuits”. In: *International Journal of Mineral Processing* (2009).
- [73] M. Zanin, I. Ametov, S. Grano, L. Zhou, and W. Skinner. “A study of mechanisms affecting molybdenite recovery in a bulk copper/molybdenum flotation circuit”. In: *International Journal of Mineral Processing* 93.34 (2009), pp. 256–266.
- [74] W. Zhang. “Water overflow rate and bubble surface area flux in flotation”. Master’s Thesis. McGill University, 2009.
- [75] W. Zhang. “Effect of Solids on Pulp and Froth Properties in Flotation”. Department of Mining and Materials Engineering, 2010.

- [76] X. Zheng and L. Knopjes. “Modelling of froth transportation in industrial flotation cells: Part II. Modelling of froth transportation in an Outokumpu tank flotation cell at the Anglo Platinum Bafokeng-Rasimone Platinum Mine (BRPM) concentrator”. In: *Minerals Engineering* 17.9-10 (2004), pp. 989–1000.
- [77] X. Zheng, J. P. Franzidis, N.W. Johnson, and E. Manlapig. “Modelling of entrainment in industrial flotation cells: the effect of solids suspension”. In: *Minerals Engineering* 18 (2004), pp. 51–58.
- [78] X. Zheng, J. P. Franzidis, and E. Manlapig. “Modelling of froth transportation in industrial flotation cells: Part I. Development of froth transportation models for attached particles”. In: *Minerals Engineering* 17.9-10 (2004), pp. 981–988.
- [79] X. Zheng, J. P. Franzidis, and N. W. Johnson. “An evaluation of different models of water recovery in flotation”. In: *Minerals Engineering* 19.9 (2006), pp. 871–882.
- [80] X. Zheng, N. W. Johnson, and J. P. Franzidis. “Modelling of entrainment in industrial flotation cells: Water recovery and degree of entrainment”. In: *Minerals Engineering* 19.11 (2006), pp. 1191–1203.

Chapter 3

Bank Profile Simulations

Recovery in flotation encompasses two processes: true flotation, where mineral is collected on the surface of a bubble; and entrainment, where mineral is hydraulically recovered in relation to the recovery of water (Engelbrecht and Woodburn 1975). For discussion purposes minerals recovered by true flotation will be referred to as ‘floatable’ minerals and can be characterised by a flotation rate constant; and minerals recovered by entrainment will be referred to as ‘entrained’ minerals. The required separation, therefore, may be between two (or more) floatable minerals and/or between floatable and entrained minerals.

Maldonado et al. (2011) developed an algorithm to examine the first case: separation of two floatable minerals, A and B, in a bank of n cells in series. The optimisation metric was to maximise the difference in recovery between A and B (or separation efficiency, $S.E. = R_A - R_B$) at a given target recovery of A. The analysis considered a bank of isolated, fully-mixed cells—which approximates the situation for a bank of mechanical cells—and assumed that the ratio of floatabilities, S , was the same for each cell in the bank, that is:

$$S = \frac{k_A}{k_B} \tag{3.1}$$

where k is the rate constant. The conclusion was that the bank should be operated with each cell having the same recovery based on the feed to the cell, i.e., a balanced or flat recovery profile. Some support for this bank operating strategy came from independent case studies (Maldonado et al. 2012).

The purpose of this chapter is to extend the analysis of Maldonado et al. (2011; 2012) to include variable S and entrainment. Rather than attempting to program new algorithms it was decided to use an existing flotation simulation package. Of

the simulators trialed, JKSimFloat was chosen as it is able to concurrently simulate various cell (machine) factors (e.g., gas hold-up and gas superficial velocity), and is widely used in industry.

The modelling of floatable mineral recovery uses the well established fully-mixed kinetic model and will not be reviewed here; rather the problem of modelling entrainment is considered.

3.1 Modelling Entrainment

As mentioned, the recovery due to entrainment is related to water recovery. The problem then becomes one of predicting water recovery. An option in JKSimFloat is to model the water overflow rate (Q_W) as a function of the solids overflow rate (Q_S) (Equation 3.2) using two fitted constants (a and b). A first estimate of the solids overflow rate is given by the floatable solids overflow rate calculated from the first order kinetic model, knowing the rate constant. The water recovery (R_W) can be calculated by dividing the water overflow rate by the water feed rate; the entrainment recovery (R_{ENT}) is proportional to the water recovery (R_W) by the entrainment factor (ENT) (Equation 3.3).

$$Q_W = aQ_S^b \quad (3.2)$$

$$R_{ENT} = ENT R_w \quad (3.3)$$

Equation 3.3 can be rewritten in terms of mass flow rates (i.e., $R = \frac{Q_{Concentrate}}{Q_{Feed}}$) to give Equation 3.4. This allows Equations 3.2 and 3.3 to be combined giving Equation 3.5, which is the entrained solids for a single flotation cell, where the entrainment constant (ENT) has been merged with the fitted constant, a (denoted as a'). While this model is empirical and possesses a simple form, it agrees with the observation that it is floatable solids that promotes froth stability and increases water recovery (Hunter et al. 2008).

$$\frac{Q_{ENT}}{Q_{Gangue,Feed}} = ENT \frac{Q_{W,Concentrate}}{Q_{W,Feed}} \quad (3.4)$$

$$Q_{ENT} = a'Q_s^b \quad (3.5)$$

The form of Equation 3.5 has an implication on how the bank should be run to minimise entrainment recovery. To illustrate the implication of using a balanced mass pull profile on Equation 3.5, consider the case where each cell has an equal mass pull, i.e., $\frac{Q_{s,Bank}}{n} = Q_{s,Cell}$. Applying this case to a bank of n cells, Equation 3.5 can be expressed as Equation 3.6, since the total entrainment from the bank is the summation of the entrainment from each cell. Equation 3.6 can be further simplified, shown as Equation 3.7.

$$Q_{ENT,Bank} = \Sigma a' \left(\frac{Q_{s,Bank}}{n} \right)^b \quad (3.6)$$

$$Q_{ENT,Bank} = \frac{Q_{ENT,SingleCell}}{n^{b-1}} \quad (3.7)$$

Zheng et al. (2006) found that b varies from 1.05 to greater than 2 for a range of cell types and operating conditions. Data collected in a 320 cm x 10.16 cm flotation column with 1 % solids by Quinn (2006) produced a value of $b = 1.43$, consistent with this range (Figure 3.1). Further data will be presented in Chapter 5 to support the general finding that $b > 1$.

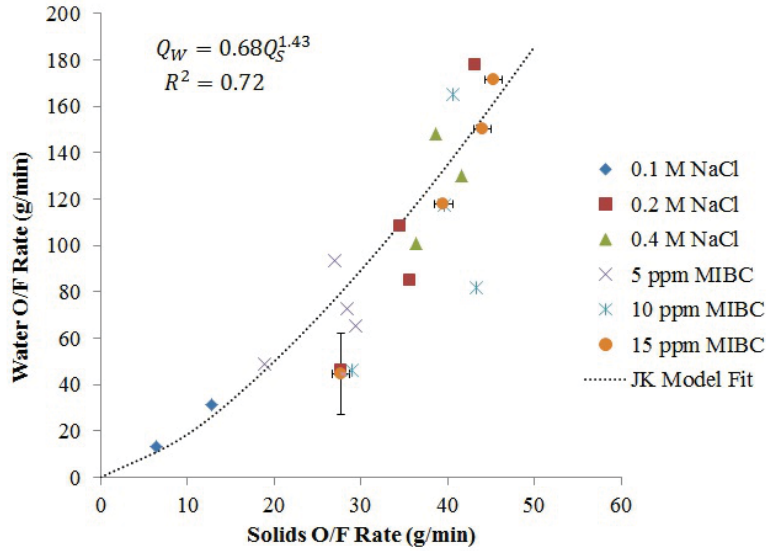


Figure 3.1: Solids and water overflow rates in a 320 cm x 10.16 cm flotation column with 1 % solids (talc). Adapted from Quinn (2006).

If $b > 1$ holds then Equation 3.7 reduces to the inequality Equation 3.8. Equation 3.8 indicates that splitting the mass flow rate of concentrate evenly to each cell down the bank gives less entrainment compared to a single (large) cell producing the same mass of concentrate (Finch 2012). From Equation 3.7, the benefit of equal mass

split increases as the value of b increases and as the number of cells (n) increases (Finch 2012). If the case $b < 1$ is considered, Equation 3.7 reduces to the inequality Equation 3.9, which implies that there is no benefit to splitting the mass down the bank. In fact if $b < 1$ it would be preferable to have a single cell.

$$\frac{Q_{ENT,Bank}}{Q_{ENT,SingleCell}} < 1 \quad (3.8)$$

$$\frac{Q_{ENT,Bank}}{Q_{ENT,SingleCell}} > 1 \quad (3.9)$$

The importance of equal mass pull can be judged qualitatively by considering the non-equal mass pull case: with $b > 1$, if a given cell over-recovers entrainment will increase—lowering the separation efficiency of that cell (i.e., lowering the difference $R_A - R_{ENT}$). This loss in separation efficiency cannot be rectified by other cells in the bank under-recovering.

The above analysis indicates that an equal mass pull from each cell (i.e., a balanced mass profile) would yield the best separation efficiency, between a floatable and an entrained mineral. Maldonado et al. (2011) found that a balanced recovery profile gives the best separation efficiency between two floatable minerals. This implies that the bank optimum would be some compromise between a balanced mass pull profile (mass pull calculated with respect to bank feed) and a balanced recovery profile (based on cell feed), depending on the ore composition, i.e., relative amount of non-target floatable mineral B and entrained mineral E. This compromise scenario will be addressed using the simulator.

3.2 Simulator Set-up

3.2.1 Flotation Parameters

JKSimFloat was set-up for a bank of four cells (Figure 3.2) considering separation of galena (target floatable mineral, A), from sphalerite (second floatable mineral, B), and entrained gangue (ENT). The initial machine parameters are not sourced from any single operation. These parameters are presented based on how they appear in JKSimFloat.

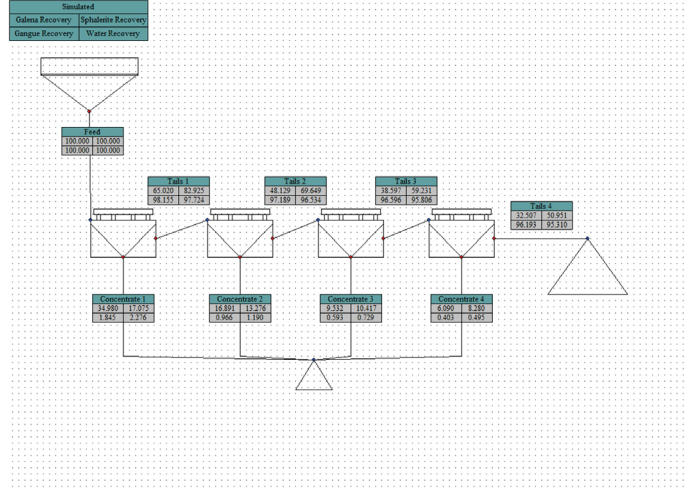


Figure 3.2: Screen shot of the JKSimFloat set-up used

The gas hold-up is defined as a linear function of the superficial gas velocity, J_g (where m and c are fitted constants) (Equation 3.10). The water overflow rate from the cell is defined as a power function dependent on the flowrate of solids (Equation 3.2).

$$\epsilon_g = mJ_g + c \quad (3.10)$$

The feed tonnage was set at 1275 tonnes per hour at 34 % solids with the ore composition (Table 3.1) taken from Welsby (2009). The distribution of floatabilities over a range of size fractions, given as P_i values in the $k_i = P_i S_b R_f$ relationship was also taken from Welsby (2009) (Table 3.2). To simplify the distinction between floatable and entrained minerals in the simulator, galena and sphalerite were assumed to have zero entrainment. The entrainment parameters by size fraction for gangue were based on silica (Smith and Warren 1989) (Table 3.3).

Table 3.1: Feed Composition for Flotation Simulations. From Welsby (2009).

Size	%of Stream	%Galena	%Sphalerite	%Gangue
+106um	15.17	1.32	2.68	96.00
-106+75um	11.70	1.32	2.68	96.00
-75+38um	9.69	5.76	8.29	85.95
-38+28um	7.50	5.76	8.29	85.95
-28+19um	8.96	12.98	8.54	78.48
-19+10um	20.84	12.98	8.54	78.48
-10um	26.14	12.98	8.54	78.48
All Size Classes		8.61	6.92	84.47

Table 3.2: Mineral Floatabilities by Size–used in Simulator Set-up. From Welsby (2009).

Label	Mineral	SG	P
+106um	Galena	7	3.68E-04
-106+75um	Galena	7	7.23E-04
-75+38um	Galena	7	1.07E-03
-38+28um	Galena	7	1.18E-03
-28+19um	Galena	7	4.96E-04
-19+10um	Galena	7	2.25E-04
-10um	Galena	7	3.00E-05
+106um	Sphalerite	4	1.17E-04
-106+75um	Sphalerite	4	1.65E-04
-75+38um	Sphalerite	4	1.58E-04
-38+28um	Sphalerite	4	1.57E-04
-28+19um	Sphalerite	4	9.28E-05
-19+10um	Sphalerite	4	4.48E-05
-10um	Sphalerite	4	2.50E-05

Table 3.3: Gangue Entrainment Factors by Size Fraction. Based on Silica modified from Smith and Warren (1989).

Mineral	+106um	-106+75um	-75+38um	-38+28um	-28+19um	-19+10um	-10um
Gangue	0.00	0.15	0.59	0.78	0.90	1.00	1.00

3.2.2 Simulation Methodology

The target bank recovery of galena (the target mineral) was set at 75 %. JKSimFloat starts by assuming that 10 % of the floatable material in the feed reports to the concentrate stream (Schwarz and Alexander 2006). With this assumption the initial water overflow to the concentrate can be calculated (Equation 3.2). Knowing the initial water and solids overflow rates, the tailing flow rate and residence time can be calculated. Entrained material is redirected from the tailings stream to the concentrate. The calculations are repeated in a loop until the mass in each particle class converges (Schwarz and Alexander 2006).

To obtain a target recovery the primary control was the bubble surface area flux, S_b (Equation 3.11):

$$S_b = \frac{6J_g}{D_{32}} \quad (3.11)$$

In a plant environment this would be analogous to changing the bubble size (D_{32}), or more practically the air rate (i.e., the superficial gas velocity, J_g) to the cell. For

froth recovery, it was assumed that the froth would be selective to galena such that $R_{f,galena} = 60\%$, $R_{f,sphalerite} = 30\%$, $R_{f,silica} = 30\%$. It was decided to fix these values as the change in S_b is more tangible, however, it is possible to create recovery and mass pull profiles using a change in R_f (this will be examined in a sensitivity analysis). It is expected that a change in R_f would be equivalent to a change in S_b as they are both constants in the $k = PS_bR_f$ relationship.

An initial net of S_b values was cast using the simulation manager until the target recovery (in terms of mineral recovery or mass pull) was obtained from the first cell. The value of S_b applied to the first cell was then fixed and the process repeated on subsequent cells. The value of S_b needed to achieve a given condition may not be practical in terms of plant operation, however this is ignored as it is the effect of recovery and mass pull profiles that matter, not how they are achieved (at least this is the working hypothesis). After the bank conditions have been identified, the simulator returns the galena/sphalerite/gangue recoveries on a size by size basis, as well as the water and solids mass overflow rates. This is done for each concentrate stream for a total of 104 results. These results are then assembled to compare the bank performance for various profiles. The performance metric chosen to compare the profiles was separation efficiency, as used by Maldonado et al. (2011), i.e., the difference between mineral recoveries. For the simulations considered the separation efficiency may be defined in three ways: between two floatable minerals (Equation 3.12), between the target floatable mineral and entrained mineral (Equation 3.13), or as an overall separation efficiency between the target floatable mineral, second floatable mineral and entrained mineral (Equation 3.14).

$$S.E. = R_A - R_B \quad (3.12)$$

$$S.E. = R_A - R_{ENT} \quad (3.13)$$

$$S.E. = R_A - R_B - R_{ENT} \quad (3.14)$$

The trial and error process of finding the correct conditions for a given profile (recovery or mass pull) was performed using Microsoft Excel as it allowed values to be incremented. Also, while JKSimFloat returns a variety of results from the simulations it does not facilitate using these results in subsequent calculations or in creating graphical representations of the data.

3.3 Tested Profiles

Six profiles are presented, which illustrate a wide range of options to achieve the same target bank galena recovery of 75 % (Table 3.4). The first five profiles are recovery profiles (recovery based on cell feed) of galena. The last profile (6) is a balanced mass pull profile (i.e., combined mass of galena, sphalerite, and gangue), with mass pull based on bank feed. The prior five recovery profiles, in turn create mass pull profiles to give the six profiles of mass pull.

Profiles 1 and 3 are stepwise increasing and decreasing profiles relative to recovery in cell 1, respectively, with subsequent cells having equal recovery to meet the target 75 % galena recovery. Profile 2 is the balanced cell by cell recovery profile. Profiles 4 and 5 are increasing and decreasing profiles, respectively, with progressive change in cell recovery (Figure 3.3).

For profile 6, balanced mass pull relative to the bank feed, the target mass pull is based on the average total mass pull of profiles 1 to 5. The corresponding recovery of galena using profile 6 is 75.02 %, facilitating comparison with profiles 1 to 5.

Table 3.4: Profiles evaluated using JKSimFloat (note, profiles 1–5 are galena recoveries based on *cell feed*; and profile 6 is mass pull based on *bank feed*.)

	Profile	R1	R2	R3	R4	Bank
1	Increasing (Step based on cell feed)	15.00	33.50	33.50	33.50	75.00
2	Balanced (Based on cell feed)	29.30	29.30	29.30	29.30	75.02
3	Decreasing (Step based on cell feed)	60.00	14.50	14.50	14.50	75.00
4	Increasing (Based on cell feed)	15.00	24.10	33.10	42.10	75.01
5	Decreasing (Based on cell feed)	60.00	23.80	13.80	4.80	74.99
6	Balanced Mass Pull (12.88% Bank Target)	2.98	2.98	2.98	2.98	11.90

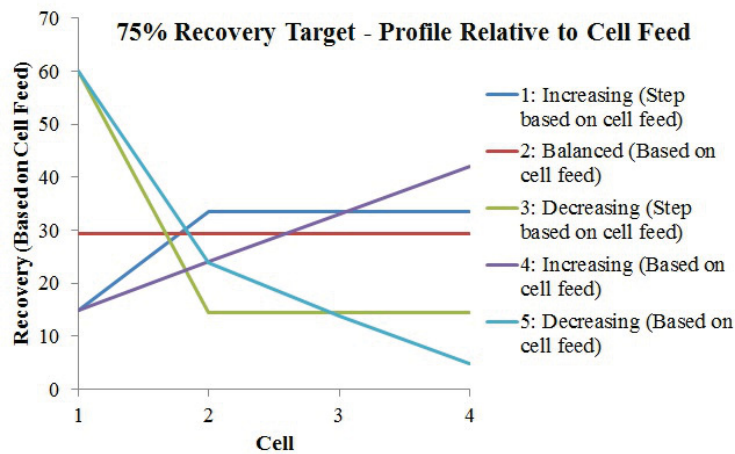


Figure 3.3: Graphical representation of profiles 1–5, galena recoveries based on the feed to each cell

It is possible to express any profile on a cell feed, or a bank feed basis. For example, a balanced recovery profile based on cell feed is an exponentially decreasing profile when considered in terms of bank feed (Appendix A). For the sake of completeness, the six profiles are also given in terms of recovery with respect to the bank (Table 3.5) as well as in terms of the total mass pull (combined mass of galena, sphalerite, and silica) from each cell, with respect to the bank feed (Table 3.6).

Table 3.5: Profiles evaluated using JKSimFloat, given in terms of bank feed. Note these profiles are the same as those in Table 3.4.

	Profile	R1	R2	R3	R4	Bank
1	Increasing (Step based on cell feed)	15.00	28.48	18.94	12.59	75.00
2	Balanced (Based on cell feed)	29.30	20.72	14.65	10.35	75.02
3	Decreasing (Step based on cell feed)	60.00	5.80	4.96	4.24	75.00
4	Increasing (Based on cell feed)	15.00	20.49	21.35	18.17	75.01
5	Decreasing (Based on cell feed)	60.00	9.52	4.21	1.26	74.99
6	Balanced Mass Pull (12.88% Bank Target)	2.98	2.98	2.98	2.98	11.90

Table 3.6: Profiles evaluated using JKSimFloat, given as mass pull based on bank feed. Note these profiles are the same as those in Table 3.4.

	Profile	M1	M2	M3	M4	Bank
1	Increasing (Step based on cell feed)	1.83	4.03	3.29	2.77	11.91
2	Balanced (Based on cell feed)	3.81	3.09	2.67	2.32	11.88
3	Decreasing (Step based on cell feed)	9.31	0.96	0.94	0.91	12.11
4	Increasing (Based on cell feed)	1.83	2.74	3.46	3.92	11.95
5	Decreasing (Based on cell feed)	9.31	1.71	0.85	0.26	12.14
6	Balanced Mass Pull (12.88% Bank Target)	2.98	2.98	2.98	2.98	11.90

3.4 The Two Floatable Mineral Case: Galena vs. Sphalerite

The results of each simulation are considered in two ways: separation efficiency of galena against sphalerite (Equation 3.12, Figure 3.4) and separation efficiency against gangue (Equation 3.13, Figure 3.6). In terms of separation efficiency against sphalerite the best performance is given by profile 2, the balanced recovery profile. The observation that a balanced profile yields the maximum separation efficiency between two floatable minerals is consistent with the conclusion drawn by Maldonado et al. (2011). The lower separation efficiencies obtained using other profiles suggest that it is detrimental to over-recover in the first cell, which is often done in practice or, for that matter, to restrain the recovery of the first cell.

While the observation agrees with the analysis of Maldonado et al. (2011) the ex-

tension is that the relative floatability, S , is not constant down the bank. The computed variation in S down the bank for each profile is shown in Figure 3.5. This calculation was done by computing the feed to each cell and obtaining a weighted average floatability, P , of galena and sphalerite¹. In all cases, including profile 2, S varies, predominantly decreasing down the bank. The balanced profile giving optimum separation efficiency appears not to depend on a constant S .

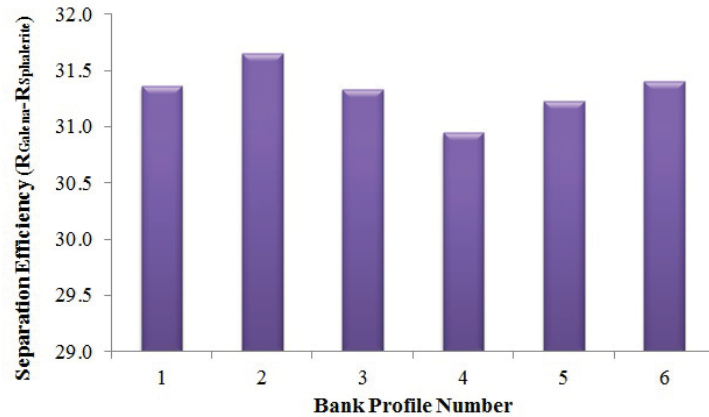


Figure 3.4: Galena-Sphalerite separation efficiency results for all simulations

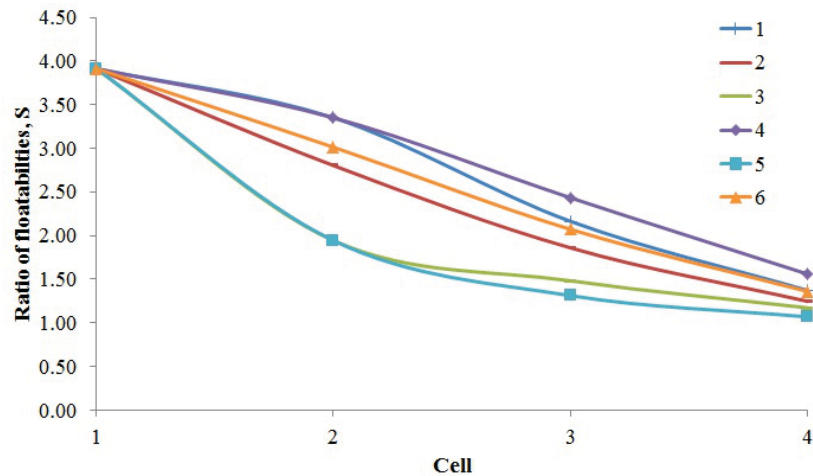


Figure 3.5: Ratio of floatabilities between galena and sphalerite (S) down the bank

¹Note, Equation 3.1 can be in terms of P since the product $S_b R_f$ is the same for both minerals

3.5 The Floatable Mineral vs. Entrained Mineral case: Galena vs. Gangue

In terms of separation efficiency against entrained gangue, Figure 3.6 supports that the balanced mass profile gives the best result, as predicted in the preliminary analysis of the JKSimFloat water overflow model (Equation 3.2). The balanced recovery profile (2) also gives a good separation efficiency result.

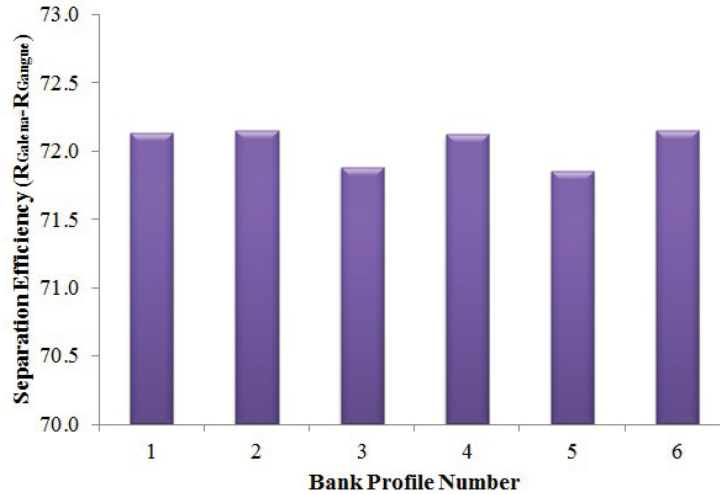


Figure 3.6: Galena-Gangue separation efficiency results for all simulations

3.6 Sensitivity Analysis

3.6.1 Effect of b

From the preliminary analysis it was postulated that the advantage of using a balanced mass pull profile would increase as the value of b increased. In Figure 3.6, profile 6, with the highest galena-gangue separation efficiency was superior to the profile with the poorest separation efficiency (profile 5) by 0.3 %. Using the same feed composition the value of b was altered for each profile in Table 3.4. The results were assessed by inspecting the difference between the separation efficiency using the balanced mass pull profile and the poorest separation efficiency given by profile 5 (Figure 3.7). In each case the best separation efficiency is given by the balanced mass pull profile and as the value of b is increased the potential gain in separation efficiency increases, suggesting that it is more important to use a balanced profile when the value of b is high.

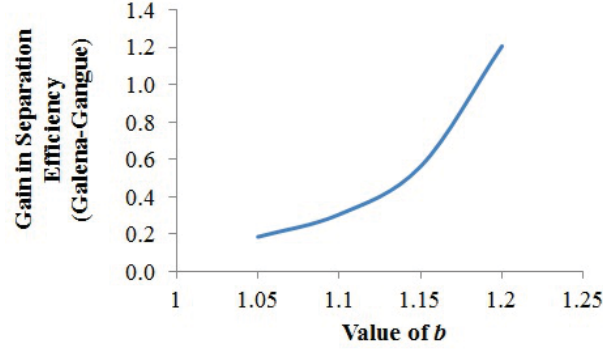


Figure 3.7: Effect of increasing the value of b on the gain in separation efficiency between galena and gangue. The gain is quantified as the separation efficiency of the balanced mass pull profile minus the lowest separation efficiency (always profile 5) defined in Table 3.4.

3.6.2 Use of Froth Recovery to Generate Profiles

The profiles (to this point) were obtained by varying S_b to obtain the bank target galena recovery. Due to the $k = PS_bR_f$ relationship, it is anticipated that R_f could be substituted for S_b as it is the product of froth recovery and bubble surface area flux that influences k .

To test this assumption, the S_b was fixed at a value of 150 s^{-1} and a change in R_f was used to create the profiles. Instead of repeating this time consuming task for all six profiles it was repeated for four cases: balanced, increasing, and decreasing recovery profiles (based on cell feed), and balanced mass pull profile (based on bank feed).

The effect of three different relative froth recoveries was also examined, by fixing the ratios between $R_{f,galena} : R_{f,sphalerite}$ and $R_{f,galena} : R_{f,silica}$ at 1, 0.5, and 0.25. In terms of separation efficiency between galena and sphalerite, the balanced recovery profile remained the best; the balanced mass pull profile again gave the highest galena–gangue separation efficiency. Using different froth recovery ratios preserves the relationship between profiles (Figure 3.8), just causing a change in the absolute separation efficiency.

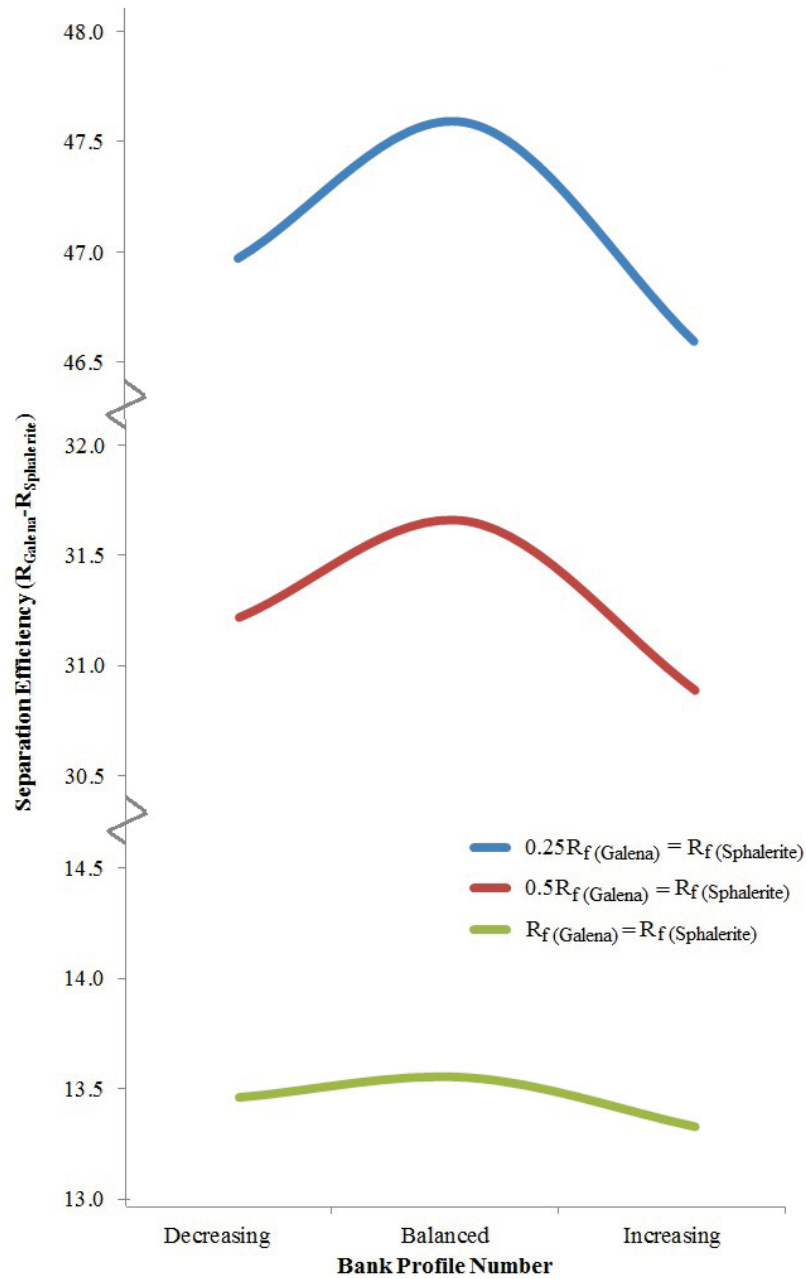


Figure 3.8: Variations in froth recovery with different ratios between mineral floatabilities

3.6.3 Compositional Changes

The idea was to try to identify a general rule when to switch the profiles from a balanced recovery (based on cell feed) to a balanced mass pull (based on bank feed) to maximise the separation efficiency between galena and both sphalerite and gangue

(Equation 3.14). In altering the composition, the galena assay in each size fraction was fixed as the original value, and the sphalerite composition was altered in set percentages between -90 % to +50 % of the original assay, so as to maintain the same sphalerite distribution by size. After the change in sphalerite composition the remainder was made up by gangue. The sphalerite recovery is always higher than that of silica, making the overall separation efficiency (Equation 3.14) an insensitive metric. In its place, the final grade at the end of the bank is considered. Figure 3.9 shows the difference in the grades obtained with a balanced recovery profile and a balanced mass pull profile as a function of sphalerite grade in the feed. The transition sphalerite grade is approximately 3.5 %: at sphalerite concentrations less than 3.5 %, the balanced mass pull profile gives a better overall bank grade (i.e., there is a negative difference between the grade using profile 2 and the grade using profile 6); and at higher sphalerite concentrations than 3.5 % the balanced recovery profile gives a better grade at the end of the bank. This supports the expectation that the feed composition will alter the choice of optimum profile.

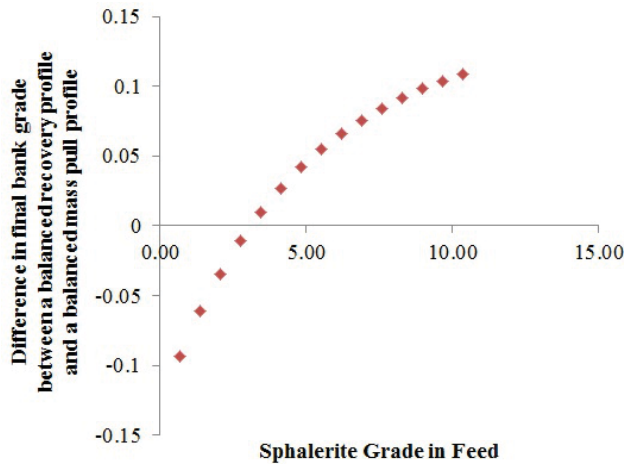


Figure 3.9: Difference in final grade between a balanced recovery and balanced mass pull profile showing the effect of varying feed composition.

3.6.4 Cell Size

The common bank arrangement is cells of equal size (volume). It is not uncommon in retrofits, however, to install a larger cell (usually at the front end) to gain capacity. The analysis by Maldonado et al. (2011; 2012) does not include cell size, with the implication it does not matter whether cells are uniform in size or not—only the recovery per cell matters. The simulator can be used to investigate if this independence of cell size holds. In the exercise the size of the first cell was doubled and each profile recreated. The results were identical to the case where each cell is

the same size: i.e., a balanced recovery profile provides superior separation against sphalerite and a balanced mass profile provides superior separation against gangue.

3.7 Discussion

The simulations presented here do not represent a general solution to the flotation optimisation problem, but they support the analytical solution of Maldonado et al. (2011) for separation of floatable minerals and the analytical solution derived for the case of separation between a floatable from an entrained mineral (Equation 3.8). The simulations aimed to extend the analysis of Maldonado et al. (2011) to include entrainment, variable S , and pulp zone/froth zone interaction (variable R_f). In considering the separation between two floatable minerals, a balanced recovery profile (based on cell feed) provides the best separation, regardless of the operating conditions, i.e., independent of variation in S and variation in froth zone recovery.

The independence from froth zone recovery is expected as the simulator uses the $k = PS_bR_f$ cell kinetic model and thus k depends on the product of S_b and R_f , and one can be traded off against the other. The effect of varying S requires a little more consideration. In the simulator, S is not directly considered but can be computed by taking a weighted estimate of k (or P) for mineral A (galena) and B (sphalerite). The result shows that S tends to decrease down the bank, which is intuitive as galena is removed faster than sphalerite (i.e., the high P galena fractions are preferentially removed). A high value of S for the first cell might imply that high recovery (higher than balanced) would exploit the large difference in mineral floatabilities. Many operations, whether by design or not, tend to pull the first cell hard as recovery is ‘easy’: the largest amount of fast floating target mineral is in the first cell. The simulations inform us this is not the best strategy. The reason is that the recovery of the second mineral (B, sphalerite) is related to the recovery of target mineral (A, galena) and the first cell incrementally recovers proportionally more sphalerite than galena and degrades the separation efficiency which the latter cells cannot undo. It is not possible to completely rule out a case where the decrease in S is so steep that some recovery above balanced in the first cell is beneficial. Changing S deliberately, as opposed to back-calculation from a given set of data (as is the case here) is difficult as it amounts to changing the floatability, P , of all the sizes in some systematic manner (i.e., changing Table 3.2). Maldonado (2012) modified their analytical solution to consider an extreme case: namely S varying from 100 to 1 as a function of the amount of mineral A recovered. They found a slight advantage in recovering more than the balanced recovery in the first three cells of a bank of seven, but concluded that a balanced recovery remained close enough

to the optimum to be the simplest operational target. Given the extreme variation in S in that analysis, this is tantamount to generalising the conclusion regarding the advantage of the balanced recovery profile being independent of variation in S over the practical range. For completeness, the opposite was also tested: S increasing from 1 to 100, which showed some benefit to above balanced recovery in the last three cells in the bank of seven, but again a balanced profile remained the practical choice.

The analysis of optimisation against entrainment using the JKSimFloat water overflow rate model (Equation 3.2) suggested that a balanced mass pull (based on bank feed) would minimise recovery due to entrainment. The simulations support that conclusion. As the value of b increases in the model the potential gain in using a balanced mass pull also increases, as predicted by Equation 3.8.

The gains in Figure 3.4 and Figure 3.6 for the optimum profile versus the other profiles are often less than 1 %, for example, in Figure 3.6, the difference between the best and worst profiles (with $b = 1.1$) is (approximately 0.3 %). This advantage may be considered too small to matter, but over the lifetime of a mine this represents a significant revenue increase. The engineer's task is to optimise circuit performance and the findings here offer a way to optimise separation efficiency in a bank by managing the distribution of cell recovery or mass pull down the bank.

The main finding is that a balanced operation of the bank, be it balanced recovery (based on cell feed) to optimise separation of floatable minerals or balanced mass pull (based on bank feed) to optimise the separation of floatable from an entrained mineral, is the best strategy. The choice of balance depends on the relative amounts of second floatable mineral recovered compared to the amount of entrained mineral. A corollary of the finding is that it is detrimental to over pull any cell, which is commonly the case with the first cell - a practice that should be resisted.

A way to identify the transition point from recovery profile dominated to mass pull profile dominated using the simulator was illustrated. Variable composition was input to identify the sphalerite grade at which the separation efficiency between galena and gangue or between galena and sphalerite is more important. Examining the final grade of the concentrate, a transition feed grade of 3.5 % sphalerite was identified: at low sphalerite concentrations a balanced mass pull gives a higher overall bank concentrate grade than the balanced recovery profile; whereas the opposite was true for sphalerite greater than 3.5 %. In principle the transition grade can be found in other cases.

An assumption in the analysis of entrainment is that $b > 1$. There is no a priori reason that this assumption always holds. However, the literature survey found no data

contrary to this assumption. The experimental sections of this thesis will examine whether there may be phenomenological support for this assumption (Chapters 5 and 6). A feature of JKSimFloat that raises a question about the calculation of entrainment is that the amount of entrained gangue in the concentrate is the result of an iterative process: the amount of gangue in one iteration ($n - 1$) is added to the next iteration (n) to calculate solids overflow rate and so on. In other words: entrainment causes subsequent entrainment, which seems a little loose on logic.

3.8 Conclusions

Simulations conducted in JKSimFloat alongside numerical analysis imply that it is detrimental to the separation efficiency of a bank to over-recover in any one cell. This confirms the analysis of Maldonado et al. (2011), which showed that a balanced recovery profile (based on cell feed) provides the best separation between two floatable minerals. The simulations showed the balanced recovery profile optimum held over a plurality of floatabilities over different size fractions.

For maximising the separation efficiency against entrainment the simulations point to a balanced mass pull from each cell based on the feed to the bank, the same solution implied after considering the JKSimFloat water overflow rate model (Equation 3.2). The benefit of using a balanced mass pull profile (i.e., the gain in separation efficiency) is sensitive to the value of b in the entrainment model.

It was assumed that the value of b in Equation 3.2 is always larger than one. Although no phenomenological reason has been suggested to support this assumption, the author has not been able to find a case where $b < 1$. The validity of this assumption needs to be further tested to confirm the analysis of this chapter.

Bibliography

- [1] J.A. Engelbrecht and E.T. Woodburn. “The effect of froth height, aeration rate and gas precipitation on flotation”. In: *Journal of South African Institute of Mining and Metallurgy* 10 (1975), pp. 125–132.
- [2] J.A. Finch. *Personal Communication*. 2012.
- [3] T.N. Hunter, R.J. Pugh, G.V. Franks, and G.J. Jameson. “The role of particles in stabilising foams and emulsions”. In: *Advances in Colloid and Interface Science* 137.2 (2008), pp. 57–81.
- [4] M. Maldonado. *Personal Communication*. 2012.
- [5] M. Maldonado, R. Araya, and J.A. Finch. “Optimizing flotation bank performance by recovery profiling”. In: *Minerals Engineering* 24.8 (2011), pp. 939–943.
- [6] M. Maldonado, R. Araya, and J.A. Finch. “An overview of optimising strategies for flotation banks”. In: *Minerals* 2 (2012), pp. 258–271.
- [7] J.J. Quinn. “Exploring the effects of salts on gas dispersion and froth properties in flotation systems”. Master’s Thesis. McGill University, 2006.
- [8] S. Schwarz and D. Alexander. *JKSimFloat V.6.1 PLUS: Improving flotation circuit performance by simulation*. 2006. URL: <http://www.jktech.com.au/sites/default/files/brochures/JKSimFloatMPMSC.pdf>.
- [9] P.G. Smith and L.J. Warren. “Entrainment of particles into flotation froths”. In: *Mineral Processing and Extractive Metallurgy Review* 5 (1989), p. 22.
- [10] S.D.D. Welsby. “On the interpretation of floatability using the bubble load”. PhD thesis. Univeristy of Queensland, 2009.
- [11] X. Zheng, J. P. Franzidis, and N. W. Johnson. “An evaluation of different models of water recovery in flotation”. In: *Minerals Engineering* 19.9 (2006), pp. 871–882.

Chapter 4

Experimental Apparatus and Procedures

Laboratory experiments were carried out to test the JKSimFloat water overflow rate model (Equation 4.1) and the assumption made in Chapter 3 that $b > 1$. If a phenomenological reason exists for $b > 1$, it would provide confirmation of the analysis conducted in Chapter 3 which showed that a balanced mass pull profile would minimise non-selective recovery due to entrainment, maximising separation efficiency against entrained gangue which translates to a higher product grade for equal recovery.

$$Q_w = aQ_s^b \quad (4.1)$$

Solids and water overflow rate data were collected in several systems: batch Denver flotation cell, laboratory flotation column, and industrial scale mechanical machines. Hydrodynamic data (bubble size, gas hold-up, and superficial gas velocity) were also collected. Talc was used in the laboratory and industrial scale experiments as a model hydrophobic solid (to ensure that the solids in the experiments floated via true flotation).

4.1 Talc Properties

4.1.1 Degree of True Flotation

The implication of the JKSimFloat water overflow rate model is that floatable solids provide the froth stability promoting water recovery. Although in the simulator a

portion of water recovery is attributed to solids recovered by entrainment, most of the solids are recovered by true flotation. To simplify the experimental system it was decided that solids should only be recovered via true flotation. It is for this reason that talc was selected as a model hydrophobic solid.

Ross (1990) developed a test to measure the degree of true flotation in a given system. While numerous other tests have been developed, the Ross test has the advantage of being simple as it requires only one test (avoiding issues based on differential conditioning of the flotation feed) (George et al. 2004). The Ross test starts by stating that the total flotation recovery (R_T) is the sum of true flotation (T) and entrainment recovery (R_e) (Equation 4.2):

$$R_T = T + R_e \quad (4.2)$$

The recovery due to entrainment is given with respect to the recovery of water (R_w), the initial concentration of mineral in the pulp (C) and the change in the mineral concentration in the pulp with time (b). The test assumes that the concentration of solids in the froth is identical to that of the pulp (i.e., there is no differential classification of water or solids at the pulp–froth interface). Flotation tests were carried out in a 1.5 L batch Denver cell at 15 % solids, with bubble size controlled using 0.4 M sodium chloride¹. Batch floats were collected at 30, 60, 90, 150, and 270 s. After the reproducibility of the system was verified, the Ross test was performed in triplicate and it was found that 85 % of the particles were recovered by true flotation with 14 % recovered by entrainment after 4.5 min (Figure 4.1). This was deemed to be an acceptable true flotation response to proceed with further tests.

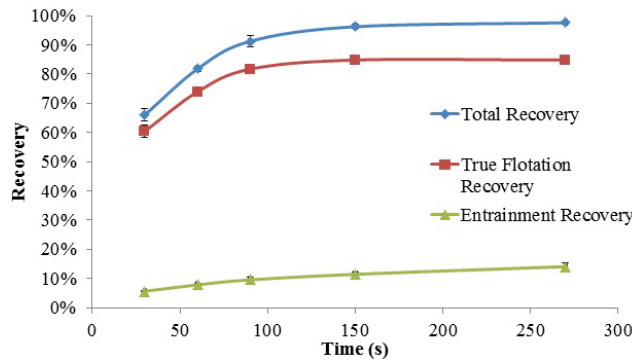


Figure 4.1: Ross test to measure the degree of true flotation for 15 % talc.

¹Salt was used because talc can adsorb some frothers

4.1.2 Composition and Size Distribution of Talc

The talc used in the laboratory experiments was supplied by a talc concentrator in Northern Ontario. The composition is given in Figure 4.2. The talc was dry screened at $-106\ \mu\text{m}$ to remove the coarse fraction (due to settling issues in the tailings line of the lab column). The particle size distribution of talc was measured using a laser particle size analyser (HORIBA LA-920)—the particle size measured by laser is larger than that measured by screening as talc particles are shaped as platelets. The size was measured before and after screening, and the resulting distribution is shown in Figure 4.3. Removing the coarse fraction did not change the particle size distribution to a large extent and it was assumed that the composition remained the same before and after screening.

After screening to remove coarse material the d_{50} (50 % passing size) increased. This result is counter-intuitive. During screening, there was a large amount of dust produced; it is possible that the loss of this fine material acted to increase the d_{50} . It is worth noting that the screening of lenticular particles is not always straight forward: it depends on the direction in which particles enter the screen.

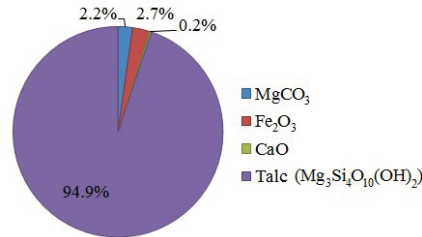


Figure 4.2: Approximate composition of the talc used in laboratory scale experiments.

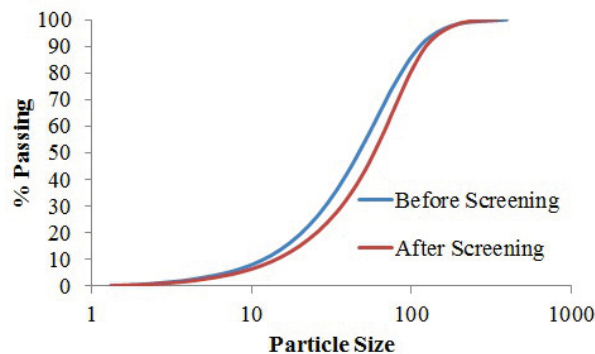


Figure 4.3: Laser particle size analysis before and after screening to remove some coarse material.

4.1.3 Reagent Adsorption

A concern using talc is the adsorption of reagents (Kuan and Finch 2010). Before and after contact tests were used to determine whether sodium chloride and 1-pentanol (alcohol frother) would adsorb on talc. The properties of the solution before and after contact were measured using either total organic carbon analysis (for 1-pentanol) or conductivity (for salt). Polypropylene glycol (PPG 400) was considered as a second frother (polyglycol type). It was assumed to adsorb based on Kuan and Finch (2010) and was used in concentrations above its critical coalescence concentration (Cho and Laskowski 2002) to allow for possible adsorption.

Table 4.1: Flotation reagents for bubble size control used in laboratory experiments.

Reagent	Supplier	Chemical Formula	Molecular Weight (g/mol)
Sodium Chloride	Fisher Scientific	NaCl	58.44
1 -Pentanol	Acros Organics	$C_5H_{12}O$	88.15
Polypropylene Glycol 400	Alfa Aesar	$H[OCH(CH_3)CH_2]_nOH$	400.00

4.2 Laboratory Overflow Tests

In a flotation system there are numerous factors which can influence the solids and water overflow rate including: bubble size, air velocity (J_g), froth depth, pulp density (% solids) and the reagent type along with several uncontrollable factors (Figure 4.4). The measurable variables from each experiment were the bubble size, gas hold-up and overflow and underflow rates.

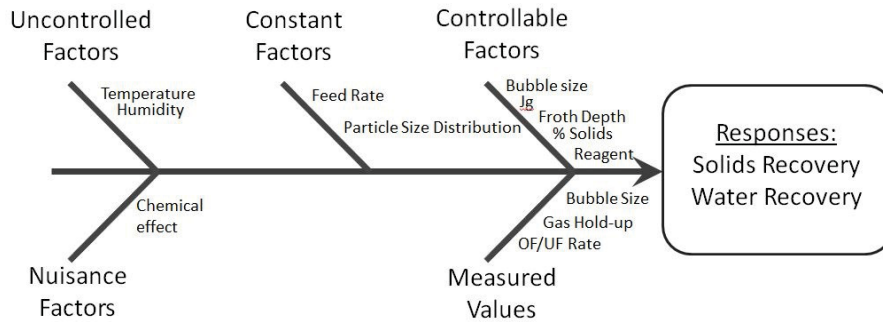


Figure 4.4: Fishbone diagram depicting factors affecting solids and water recovery from a flotation cell

4.2.1 Denver Cell Experiments

Batch Denver cell flotation tests have the advantage of being simple, however the set-up makes it difficult to measure the gas hold-up and bubble size. It is also difficult to vary the level in a systematic way (it is usually set by the volume of liquid in the cell). With these considerations in mind, a design of experiment (DOE) was created to determine the effect of air rate and solids concentration (% solids) on overflow rate. The tests were done in a Box-Wilson central composite design with centre point repeats (Figure 4.5). The basic design of experiment tests different levels of factors (a square design in the case of two factors), to which a Box Wilson design assigns centre points and levels outside the square. In this way, non-linear trends may be observed in the resulting data. Batch floats were taken at 30, 30, 30, 60, and 120 *s* intervals.

This experimental design (Table 4.2) was repeated for the three reagents listed in Table 4.1: sodium chloride, 1-pentanol, and polypropylene glycol 400.

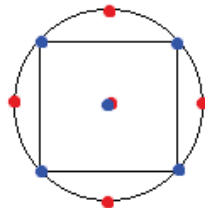


Figure 4.5: Schematic of a Box Wilson design showing the basic factorial design (in blue) and the circles ascribed by the Box Wilson design (in red).

4.2.2 Laboratory Column Experiments

To collect overflow data in a different system a lab column cell was used (Figure 4.6) with varying percent solids and overflow rates (controlled via level). The experiments were conducted at 30 *ppm* 1-pentanol.

Table 4.2: Design of Experiment used to test the effect of solids concentration and air rate in a Denver cell

Reagent	Concentration	
PPG 425	25 ppm	
Pentanol	30 ppm	
Sodium Chloride	0.35 M	
Total Cell Volume	1.2 L	

Test	Air rate (LPM)	% Solids
1	1.5	5
2	1.5	15
3	7.0	5
4	7.0	15
5	4.2	10
6	4.2	10
7	0.4	10
8	8.1	10
9	4.2	17
10	4.2	3

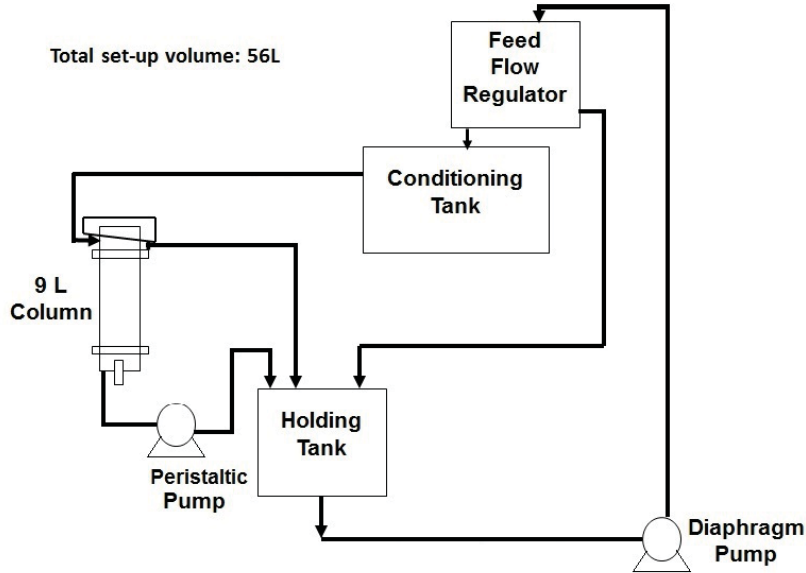


Figure 4.6: Schematic of the set-up used for the laboratory column tests. Modified from Zhang (2010).

The column was found to ‘boil’ at $J_g > 1.5 \frac{cm}{s}$. Because of this restricted range, air rate was not used to change the overflow rate, but rather the underflow rate (froth depth) was used. Bubble size was measured using the McGill Bubble Viewer and gas hold-up, using water manometers. Care was taken not to allow solids to enter the manometer lines to maintain a constant fluid density in the line.

The overflow rate was altered by varying the speed of the peristaltic underflow pump. The feed to the cell was kept at $1700 \frac{g}{min}$ for the 0.5, and 1 % solids tests and $2300 \frac{g}{min}$ for the 2, and 5 % solids tests using the distributor shown in Figure 4.6. The higher feed rate was used for the higher percent solids to avoid particle settling in the distributor. Four to five underflow rate speeds were set for each solids concentration tested (0.5, 1, 2, and 5 % solids). The pump speeds were selected visually to allow for the widest range of overflow rates: for example if the rate was too low the solids would not flow readily through the overflow line, biasing the sample. A mass balance was conducted as a check on the system and is shown in Appendix B.

McGill Bubble Viewer

Bubble size measurements were taken using the McGill Bubble Viewer (Figure 4.7). Bubbles are directed into a backlit chamber where photographs are taken (Figure 4.8). The photographs are analysed using a routine in imaging software (Empix Imaging Inc 2007). At least 1000 bubbles are considered to arrive at an average bubble size.

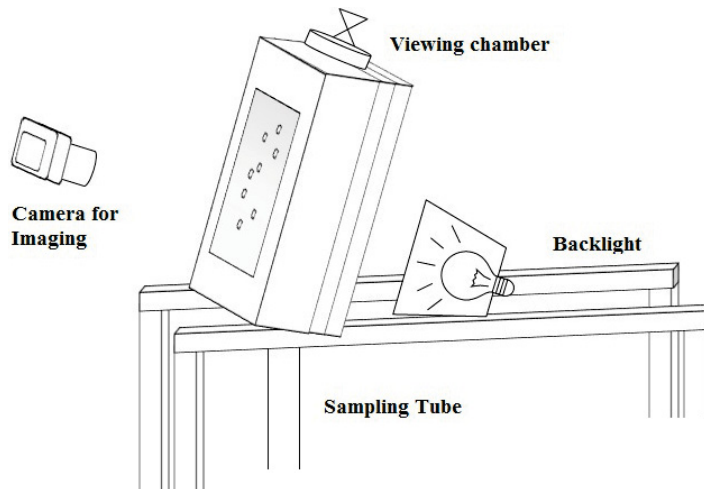


Figure 4.7: Schematic of the McGill Bubble Viewer used for sampling.

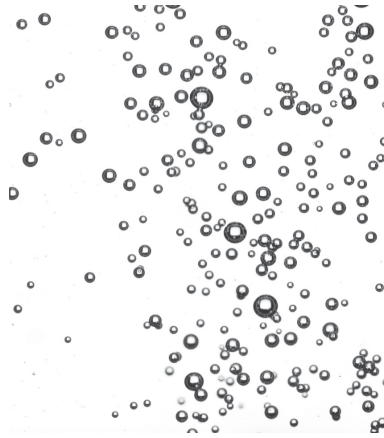


Figure 4.8: Sample bubble size image for processing in Northern Eclipse.

Gas Hold-up Measurements

The gas hold-up in the cell was measured using water manometers mounted to the column wall with 49 *cm* between taps. The gas hold-up is given by the difference in water level between the two manometers divided by the distance between them (Equation 4.3):

$$\epsilon_g = \frac{\Delta P}{\text{Distance between taps}} \quad (4.3)$$

4.2.3 Industrial Tests

As part of a sampling campaign at a talc concentrator in Northern Ontario, overflow samples were collected from cells in the rougher bank (Figure 4.9) as well as in the cleaner and scavenger cells. The cells were 10 m^3 and less, manufactured by Outotec. Alongside overflow measurements, bubble size was also taken using the McGill Bubble Viewer, which was adapted to measure gas velocity (by timing the descent of the liquid in the viewer). The overflow samples were collected, filtered, and dried to obtain the mass of solids and liquid. The composition of the talc is different from that used in the laboratory experiments (lower purity)—the bank feed is approximately 50 % talc. Froth velocity measurements were obtained by measuring the time it took for a piece of plastic twine to travel from the centre of the cell (or edge of the froth crowder) to the lip of the cell. The bubble size and froth velocity results will be used in Chapter 6 to fit the overflow rate data to the water overflow rate model of Neethling et al. (2003).

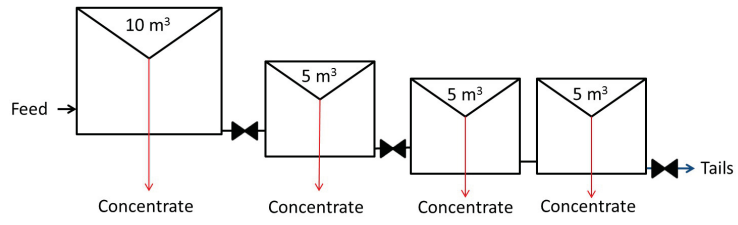


Figure 4.9: Schematic of the rougher bank on which samples were collected.

Bibliography

- [1] Y. S. Cho and J. S. Laskowski. “Effect of flotation frothers on bubble size and foam stability”. In: *International Journal of Mineral Processing* 64.23 (2002), pp. 69–80.
- [2] Empix Imaging Inc. *Northern Eclipse*. 2007. URL: <http://www.empix.com/>.
- [3] P. George, A. V. Nguyen, and G. J. Jameson. “Assessment of true flotation and entrainment in the flotation of submicron particles by fine bubbles”. In: *Minerals Engineering* 17.78 (2004), pp. 847–853.
- [4] S.H. Kuan and J.A. Finch. “Impact of talc on pulp and froth properties in F150 and 1-pentanol frother systems”. In: *Minerals Engineering* 23.1113 (2010), pp. 1003–1009.
- [5] S. J. Neethling, H. T. Lee, and J. J. Cilliers. “Simple relationships for predicting the recovery of liquid from flowing foams and froths”. In: *Minerals Engineering* 16.11 (2003), pp. 1123–1130.
- [6] V. E. Ross. “Flotation and entrainment of particles during batch flotation tests”. In: *Minerals Engineering* 3.34 (1990), pp. 245–256.
- [7] W. Zhang. “Effect of Solids on Pulp and Froth Properties in Flotation”. Department of Mining and Materials Engineering, 2010.

Chapter 5

Results

The overflow rate data collected from the batch Denver cell, laboratory column, and industrial scale machines are used to determine if one relationship can fit the data from various systems. In particular the data are used to investigate the assumption made in Chapter 3 that the value of b in the JKSimFloat water overflow rate model is always larger than one. The analysis in Chapter 3 concluded that if b is always larger than one, a bank of flotation cells should be operated with a balanced mass pull from each cell to minimise entrainment. Thus the $b > 1$ assumption is central to this conclusion and needs to be tested.

5.1 Denver Cell

A statistical design of experiment (Box Wilson design) was used to examine the effect of two factors (percent solids and air flow rate) on the solids and water overflow rate. The experimental design was repeated for the three reagents listed in Table 4.2. The results of each experiment were analysed using DOEPro (SigmaZone 2013), which returns the most important factors and how well a model of those factors fits the data (Y-hat model) as well as the variation in data (S-hat model). The responses used were the solids and water overflow rate from the first 30 s of flotation (Table 5.1).

These data were input to DOEPro together, as if the experiment were replicated three times. Figure 5.1 shows the results obtained. In the Y-hat model, the most important factors are the air rate and solids concentration, which give an R_{adj}^2 of 0.769 for the solids overflow rate and R_{adj}^2 of 0.625 for the water overflow. Of greater interest is the S-hat model, which is a model of variability. In the S-hat model, only the solids concentration is considered to be an important factor. Most

of the variation in solids overflow and much of the variation in water overflow rate is explained by the solids concentration, with an R_{adj}^2 of 0.829 for solids and R_{adj}^2 of 0.624 for the water overflow rate.

Table 5.1: Overflow data for the first 30 seconds of Denver cell flotation.

Experiment	1	2	3	4	5	6	7	8	9	10
% Solids	5 %	5 %	15 %	15 %	10 %	10 %	10 %	10 %	17 %	3 %
Air <i>LPM</i>	1.5	7	1.5	7	4.25	4.25	8.12	0.37	4.25	4.25
NaCl										
Solids O/F ($\frac{g}{s}$)	1.0	1.4	3.3	4.7	3.1	2.5	3.1	2.2	5.4	0.7
Water O/F ($\frac{g}{s}$)	1.6	2.4	6.4	9.5	5.2	4.3	6.0	3.3	10.9	0.9
Pentanol										
Solids O/F ($\frac{g}{s}$)	1.2	1.5	3.1	5.0	2.6	3.0	2.8	2.0	5.1	0.7
Water O/F ($\frac{g}{s}$)	2.9	4.2	5.9	12.0	4.3	7.3	4.6	3.5	9.6	2.2
PPG 400										
Solids O/F ($\frac{g}{s}$)	1.2	1.5	1.8	3.4	2.1	1.8	2.5	1.3	2.7	0.8
Water O/F ($\frac{g}{s}$)	2.0	3.9	2.9	6.9	3.2	2.8	4.1	2.2	4.4	2.2

The reproducibility (i.e., the centre point repeats from the design of experiment) can be considered for the three reagents tested (Appendix B). The recovery–time curve for PPG 400 is inconsistent with those of 1–pentanol and sodium chloride. This is likely due to a different froth removal speed as the PPG 400 tests were conducted several months after the 1–pentanol and sodium chloride tests.

However, it is possible to plot all the data collected (Figure 5.2). A power function (i.e., the JK SimFloat overflow rate model) fits the data, regardless of the type of reagent used. The model is shown with the 95 % confidence interval, based on the standard error of the water overflow rate. The value of b in the model is greater than one.

Y-hat Model		Solids Overflow				Water Overflow			
Factor	Name	Coeff	P(2 Tail)	Tol	Active	Coeff	P(2 Tail)	Tol	Active
Const		2.515	0.0000			4.508	0.0000		
A	Air Rate	0.41540	0.0033	1	X	1.054	0.0055	1	X
B	%Solids	1.211	0.0000	1	X	2.260	0.0000	1	X
AB		0.33369	0.0753	1	X	0.77633	0.1250	1	X
AA		-0.09252	0.5881	0.8184	X	-0.14298	0.7579	0.8184	X
BB		0.01250	0.9415	0.8184	X	0.39703	0.3952	0.8184	X
	R ²	0.8145				0.6994			
	Adj R ²	0.7758				0.6367			
	Std Error	0.6217				1.6917			
	F	21.0730				11.1656			
	Sig F	0.0000				0.0000			
	F _{10r}	0.2249				0.5898			
	Sig F _{10r}	0.8780				0.6285			
	Source	SS	df	MS		SS	df	MS	
	Regression	40.7	5	8.1		159.8	5	32.0	
	Error	9.3	24	0.4		68.7	24	2.9	
	Error _{Full}	9.0	21	0.4		63.3	21	3.0	
	Error _{10r}	0.3	3	0.1		5.3	3	1.8	
	Total	50.0	29			228.5	29		

S-hat Model		Solids Overflow				Water Overflow			
Factor	Name	Coeff	P(2 Tail)	Tol	Active	Coeff	P(2 Tail)	Tol	Active
Const		0.53861	0.0054			1.629	0.0093		
A	Air Rate	-0.02845	0.5946	1	X	0.16638	0.3917	1	X
B	%Solids	0.43357	0.0009	1	X	0.82475	0.0089	1	X
AB		0.02899	0.6983	1	X	0.07671	0.7698	1	X
AA		-0.11821	0.1447	0.8184	X	-0.37134	0.1817	0.8184	X
BB		0.09537	0.2182	0.8184	X	0.24208	0.3519	0.8184	X
	R ²	0.9562				0.8822			
	Adj R ²	0.9014				0.7348			
	Std Error	0.1392				0.4898			
	F	17.4550				5.9884			
	Sig F	0.0080				0.0538			
	F _{10r}	5.2471				0.0708			
	Sig F _{10r}	0.3081				0.9671			
	Source	SS	df	MS		SS	df	MS	
	Regression	1.7	5	0.3		7.2	5	1.4	
	Error	0.1	4	0.0		1.0	4	0.2	
	Error _{Full}	0.0	1	0.0		0.8	1	0.8	
	Error _{10r}	0.1	3	0.0		0.2	3	0.1	
	Total	1.8	9			8.1	9		

Figure 5.1: Results returned by DOEPro for the Denver experiment results shown in Table 5.1

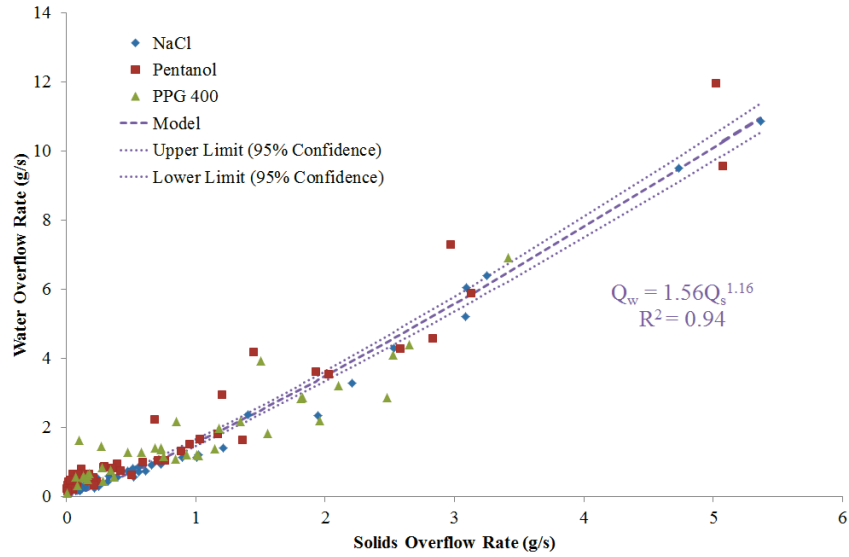


Figure 5.2: Solids and water overflow rates for the Denver cell experimental results shown in Table 5.1

5.2 Laboratory Column

In the column, overflow rate data were collected at varying talc concentrations (0.5, 1, 2, and 5 % talc). The gas hold-up and bubble size were fairly constant over each experiment and varied little with solids concentration (Table 5.2).

Table 5.2: Average bubble size and gas hold up data in the column

Gas Hold-up		Bubble Size (D_{32})	
Average	4.31%	Average	0.88 mm
Standard Deviation	0.56%	Standard Deviation	0.035 mm
Number of Samples	17	Number of Samples	4

The overflow rate data are shown in Figure 5.3. The models depend on the % solids; each solids concentration condition was fit using the JK model. The error bars on each data point represent the propagation of error on the measured values. The samples taken were composite samples so the average and standard deviation cannot be used. The value of b in each case is larger than one.

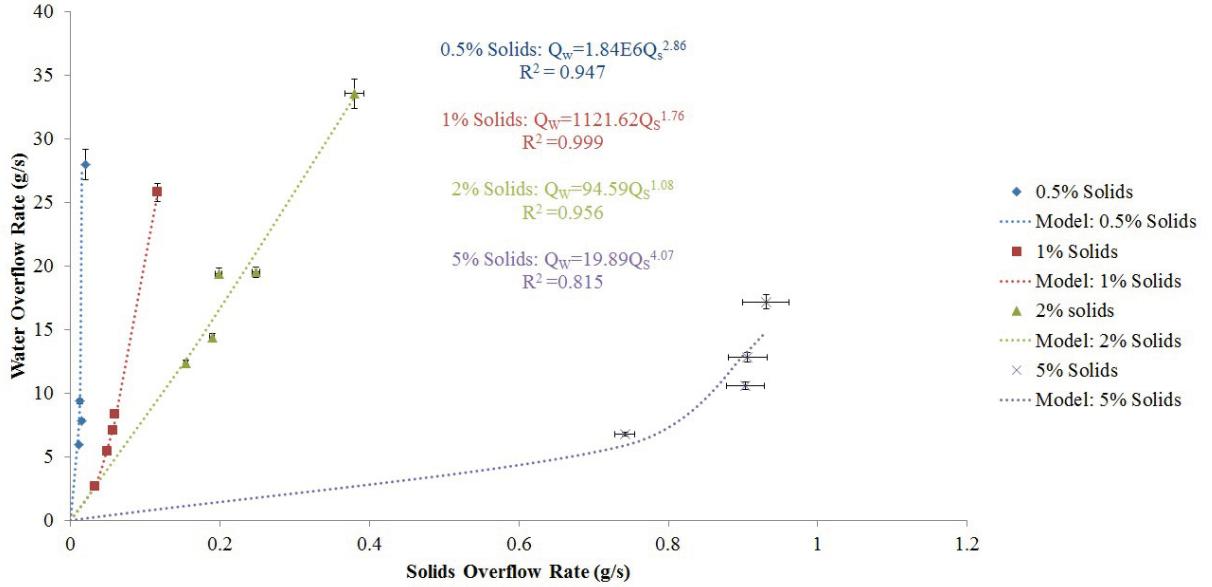


Figure 5.3: Overflow rates obtained using the miniature column system at increasing solids concentrations of talc.

5.3 Industrial Cells

It is possible to fit all of the data collected to a single power function (Figure 5.4), where the value of b is bigger than one. The data may also be divided based on banks: the rougher bank (Figure 5.5) and the cleaner bank (Figure 5.6). The fit (R^2) improves when the banks are fit separately. In each case $b > 1$ is found, although the value is close to 1.

As part of the plant campaign, two air profiles were tested on the rougher bank. Bubble size and froth velocity were measured in addition to the overflow rates. The Sauter mean bubble diameters (d_{32}) for the two profiles are shown in Figure 5.7. The froth velocity data are given in Table 5.3. Froth velocity was observed to increase down the bank of cells. The data collected in this part of the plant trial will be used in Chapter 6 to compare different models over the rougher bank.

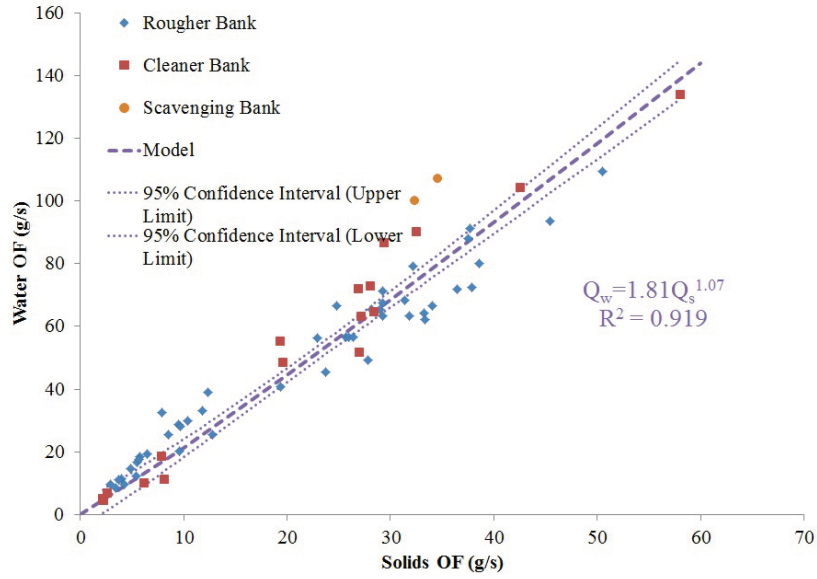


Figure 5.4: Overflow rates in the roughing, cleaning, and scavenging banks.

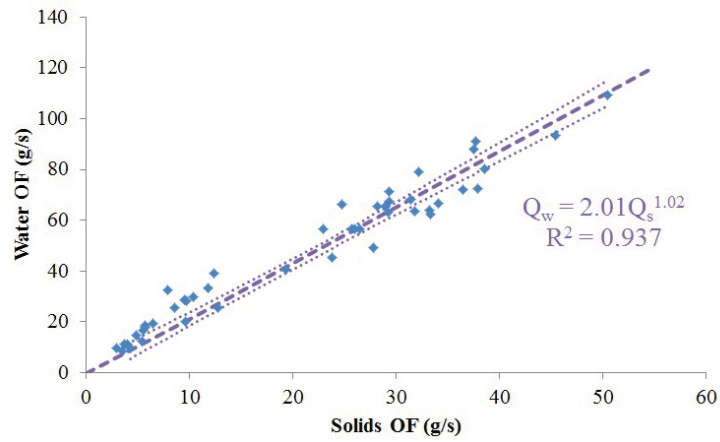


Figure 5.5: Overflow rates in the roughing bank.

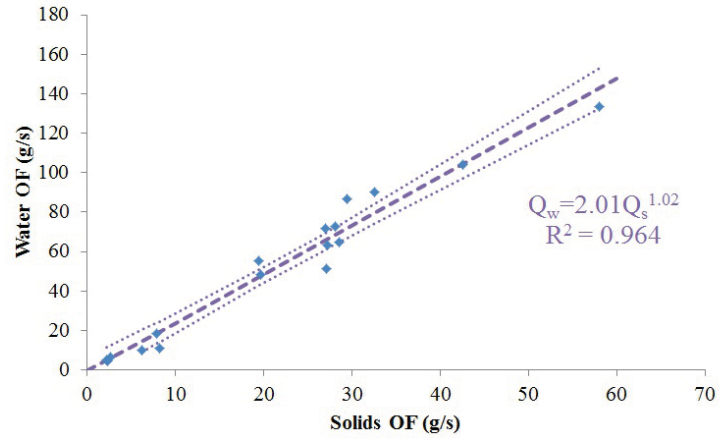


Figure 5.6: Overflow rates in the cleaning banks.

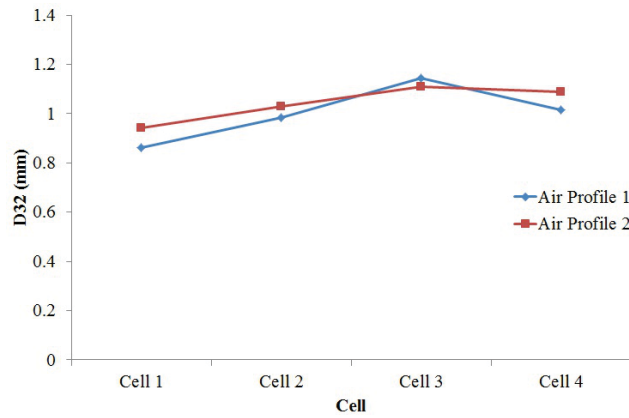


Figure 5.7: Sauter mean bubble size in the roughing bank.

Table 5.3: Measured Froth Velocities measured for the two air profiles tested.

	Cell 1	Cell 2	Cell 3	Cell 4
Air Profile 1	1.64 $\frac{cm}{s}$	2.91 $\frac{cm}{s}$	3.62 $\frac{cm}{s}$	3.38 $\frac{cm}{s}$
Air Profile 2	1.59 $\frac{cm}{s}$	3.71 $\frac{cm}{s}$	4.70 $\frac{cm}{s}$	4.11 $\frac{cm}{s}$

Bibliography

- [1] SigmaZone. *DOEPro XL*. 2013. URL: <http://sigmazone.com/doepro.htm/>.

Chapter 6

Discussion

Chapter 5 analysed the water and solids overflow rate data with respect to the JKSimFloat water overflow rate model for varied systems: batch Denver, lab column, and industrial mechanical cells. In each system the water overflow rate data could be fit using a power function model with the exponent value (b) always greater than one. The analysis suggested that a balanced mass pull profile will result in lower entrainment recovery for a given bank of cells (with equivalent pay mineral recovery). However, failing to find a case where $b < 1$ does not infer that $b > 1$ in every case. This chapter aims to compare different models for commonality and whether any machine factors can be linked to the value of b to provide phenomenological support that $b > 1$.

6.1 Alternative Water Overflow Rate Models

While the fit (R^2) was good for each set of experimental data the JKSimFloat model is only useful after the empirical parameters have been established and the model cannot be transported from one type of equipment to another. It was possible to obtain a better fit to the data by considering the roughing and cleaning banks separately, a finding shared with Zheng et al. (2006). The JKSimFloat water overflow rate model is empirical with limited predictive power, making a phenomenological model desirable. Furthermore, from a modelling perspective, power and exponential models are usually only valid over very specific ranges.

Of the seven water overflow rate models studied by Zheng et al. (2006) a simplification of a phenomenological model developed by Neethling and Cilliers (2003) was deemed to be superior as it contains only machine parameters (and would therefore have the greatest degree of predictive power). The Neethling et al. (2003) model

depends on the fraction of air recovered as unburst bubbles that overflow the cell, α (Equation 6.1):

$$\alpha = \frac{v_{froth} h_{lip} l_{lip}}{Q_{air}} \quad (6.1)$$

where v_{froth} is the froth velocity overflowing the lip; h_{lip} is the height of the froth above the lip; l_{lip} is the length of the lip; and Q_{air} is the volumetric flowrate of air in the cell. In general the value of α is less than 0.5 in flotation systems (Neethling et al. 2003). In this case, the water overflow rate (Q_w) is defined as (Equation 6.2):

$$Q_w = \frac{A_{cell} J_g^2 \lambda}{k_1} (1 - \alpha) \alpha \quad (6.2)$$

where A_{cell} is the cross-sectional area of the flotation cell; J_g is the superficial gas velocity; λ incorporates the bubble size at the top of the froth, $\lambda = \frac{6.81}{d_b^2}$; and k_1 is a constant that balances the density and viscosity of the interbubble slurry (Equation 6.3):

$$k_1 = \frac{\rho g}{3C_d \mu} \quad (6.3)$$

where ρ is the density of the interbubble slurry; g is the gravitational constant; C_d is the dimensionless viscous drag coefficient between bubbles, with a value of 49 in most flotation froths (Neethling et al. 2003); and μ is the viscosity of the interbubble slurry. While it is difficult to estimate the value of μ for a slurry it can be predicted using the volumetric fraction of solids in the slurry (ϕ) as per Mou and Adelman (1978) (Equation 6.4):

$$\mu_{slurry} = \mu_{water} (1 + 2.5\phi + 4.375\phi^2) \quad (6.4)$$

Equation 6.4 was found to underestimate the viscosity change with increasing volumetric fraction of solids (Mou and Adelman 1978) especially at high solids fractions when particle-particle interactions become significant. Other relationships for approximating viscosity assume the presence of spherical particles, which is not true for a talc system. Equation 6.4 was deemed to be sufficient to provide an order of magnitude approximation for viscosity in the Neethling et al. (2003) model.

While the data was not initially collected with the Neethling et al. (2003) model in mind, it may be possible to fit the data to this model. The parameters that were not directly measured were the velocity of the froth crossing the lip (instead the

velocity of the froth across the top of the cell was measured); the height of the froth above the lip (which was estimated from later measurements); and the value of the bubble size at the top of the froth (the measured bubble size was sampled from the pulp of the cells). Ata et al. (2003) observed that the bubble size coarsened to a lesser degree in the presence of hydrophobic particles; using a small bubble size in the model is expected to result in over-predicting the water overflow rate.

The calculations for the Neethling et al. (2003) model are provided in Appendix C. The calculated water overflow rate values were compared to the average measured values (Figure 6.1). Unexpectedly, the slope of the calculated against the measured values is negative. For a well-modelled system the value of the slope is expected to be one (i.e., the model is able to perfectly predict the calculated values). With the assumptions made regarding some values it was expected that the slope might be different from one, but that the slope would be positive (i.e., the predicted values would be in the correct direction).

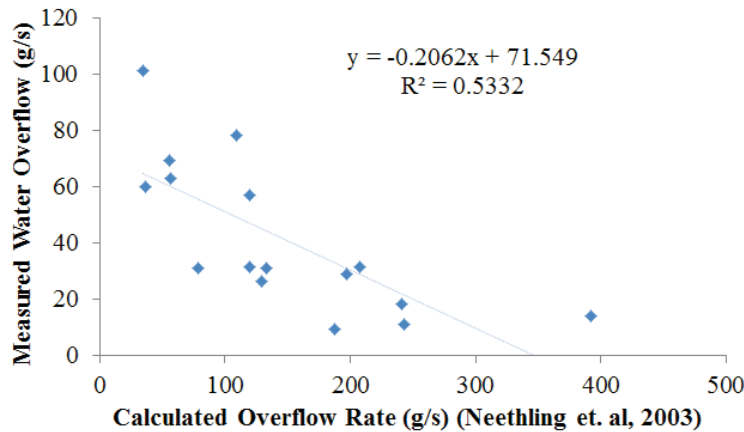


Figure 6.1: Water overflow rates predicted by the Neethling et al. (2003) model compared to measured values.

The answer to this discrepancy seems to be in the relationship between froth velocity and the total measured overflow rate (Figure 6.2): as the froth velocity increases (down the bank of cells) the overflow decreases. However, in the Neethling et al. (2003) model, as the froth velocity increases, α also increases (as the term $(1 - \alpha)\alpha$), predicting a greater amount of water overflowing the cell. The air rate also increased down the bank, which would tend to decrease the value of α .

Two physical reasons might proffer an explanation: the froth velocity measured at the lip would yield a different trend and/or the presence of talc may be causing high froth stability, resulting in a highly loaded froth with low mobility. Considering the latter, greater values of froth stability have been attributed to the presence

hydrophobic particles (Ata et al. 2003). In the case of the former, the froth velocity was observed to increase near the lip of the cell, although it is difficult to determine from a qualitative observation whether the froth velocity at the lip was increasing or decreasing down the bank.

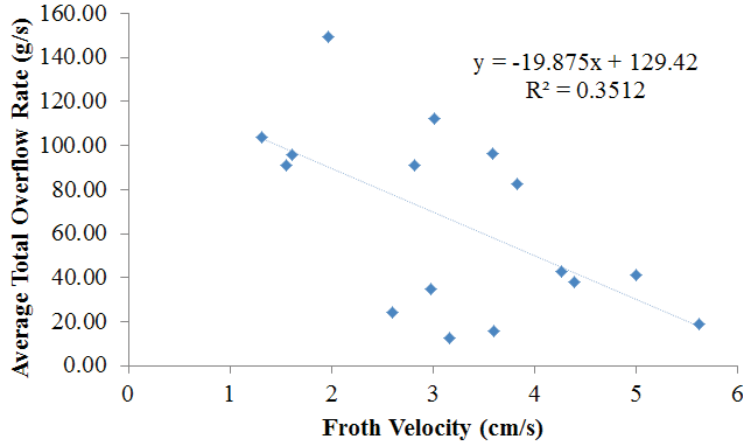


Figure 6.2: Variation in overflow rate with froth velocity for the rougher bank.

6.2 Froth Residence Time

With the available data, the Neethling et al. (2003) model could not be fit to the data collected. Further, there is no straightforward way to rearrange the Neethling et al. (2003) model in a manner that might suggest a value of b based on machine parameters. It has been suggested that the froth recovery (R_f) is exponentially related to the froth residence time, τ_f (Equation 6.5) (Gorain et al. 1998):

$$R_f = e^{-\beta\tau_f} \quad (6.5)$$

However, the value of τ_f multiplied by some constant cannot be substituted for b as the use of a constant would effectively ‘fudge’ the value to fit the data. Moreover, the value of b in a power function should be dimensionless. Considering only the froth residence time would yield units of s . The following form of the constant b is proposed (Equation 6.6):

$$b = \frac{J_g\tau_f}{H_f} \quad (6.6)$$

The froth residence time was taken to be the average residence time of air and solids

in the froth, defined by Zheng et al. (2006) to account for bubble breakage using α as defined by Neethling et al. (2003) (Equation 6.7):

$$\tau_f = \frac{\epsilon_{g,f} V_f}{\alpha Q_{air}} \quad (6.7)$$

where $\epsilon_{g,f}$ is the gas hold-up in the froth; and V_f is the froth volume. As the value of the gas hold-up was not measured it was fixed at 85 %.

If Equation 6.7 is multiplied by $\frac{A_{cell}}{A_{cell}}$, then Equation 6.6 reduces to Equation 6.8:

$$b = \frac{\epsilon_{g,f}}{\alpha} \quad (6.8)$$

Substitution of Equation 6.8 into the JKSimFloat water overflow rate model gives Equation 6.9:

$$Q_W = a Q_S^{\frac{\epsilon_{g,f}}{\alpha}} \quad (6.9)$$

The two air profiles were trialled twice on the rougher bank, resulting in four measurements of froth velocity per cell. Since multiple overflow measurements were taken at each condition, they were averaged to obtain 4 data points per cell. A value of b was tabulated for each experimental point. To examine the predictive power, the average value of b was taken for each cell (Table 6.1). Solver was used to fit a value of a for each cell (Equation 6.9) (Table 6.1). While the values of a fitted by solver are outside of the range measured thus far, the important fact is that they are non-negative values such that water overflow maintains an increasing relationship with solids overflow.

The predicted water overflow was plotted against the average measured values (Figure 6.3), which yielded a slope of one and an R^2 of 0.861, which implies a good degree of predictability.

Table 6.1: Values of a and b fitted by solver and tabulated using Equation 6.8 respectively

Cell	1	2	3	4
a	0.309	0.003	0.020	0.006
b	1.510	2.869	3.142	4.622

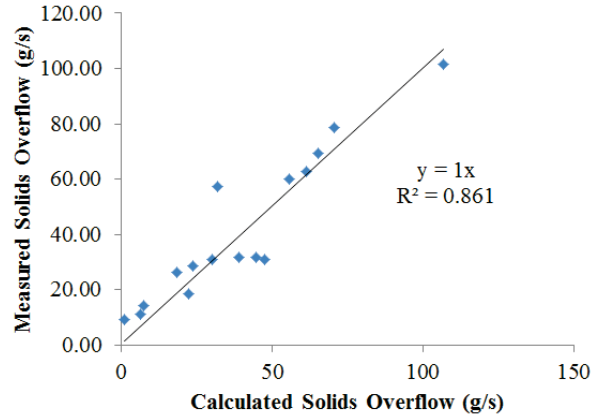


Figure 6.3: Water overflow rates predicted by Equation 6.8 compared to measured values.

This method of fitting the data resulted in one model for each cell; when plotting the rougher data (not averaged) on a cell by cell basis, it appears that each cell could fall on a separate curve (Figure 6.4). The fit for cells 1 and 4 are acceptable, however the model predicts the data poorly for cells 2 and 3.

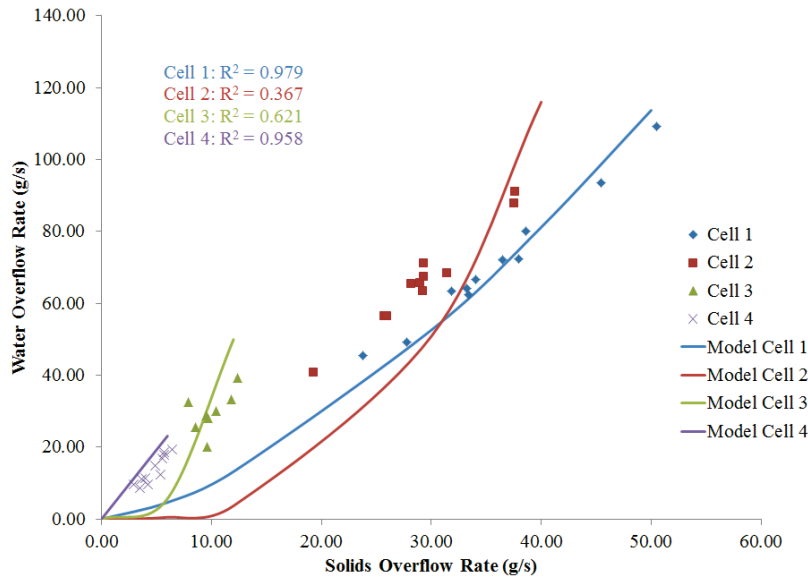


Figure 6.4: Overflow models defined by Equation 6.9 (Table 6.1) for each cell of the rougher bank.

Fitting the data on a cell by cell basis raises the question of whether four different models can yield a single power function as all of the data in Figure 6.4 were fit using a single power function in Figure 5.5. To test this, the solids overflow data and the four models were used to generate predicted water overflow rates for each cell. The results from the four models were then fit to a single power function (Figure 6.5).

While the R^2 of this function is relatively low (0.771) it is possible to conceptualise how four different data sets could be represented by a single function.

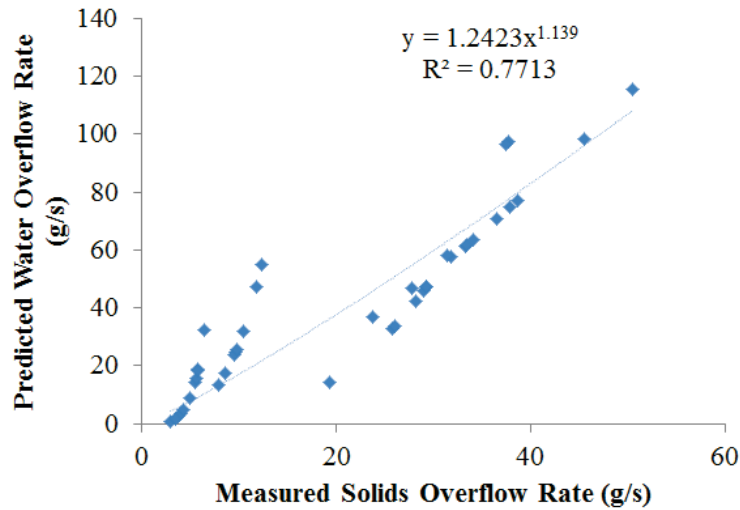


Figure 6.5: Predicted water over flow rates (Equation 6.8) for the measured solids overflow rates.

Showing Equation 6.9 fits the plant data is not the same as proving b contains those parameters, and the equation form should be tested on other systems to check for generality. The implication is that the data would be sensitive to the measured value of gas hold-up in the froth in each cell.

However, if Equation 6.9 does represent the value of b it is possible to speculate on the implications in the context of Chapter 3. As mentioned, the value of α is less than 0.5 for most flotation systems (Neethling et al. 2003). This means that as long as the value of gas hold-up in the froth is greater than 0.5, the value of b will always be greater than one. A study examining gas hold-up in froths was conducted by Tavera et al. (1998) who found that in a two-phase froth, the gas hold-up ranged from 0.6 at the froth interface to above 0.9, 100 *cm* away from the interface (Figure 6.6). With this range of values for gas hold-up in the froth, there is a strong suggestion that the value of b in Equation 6.8 will always be greater than one.

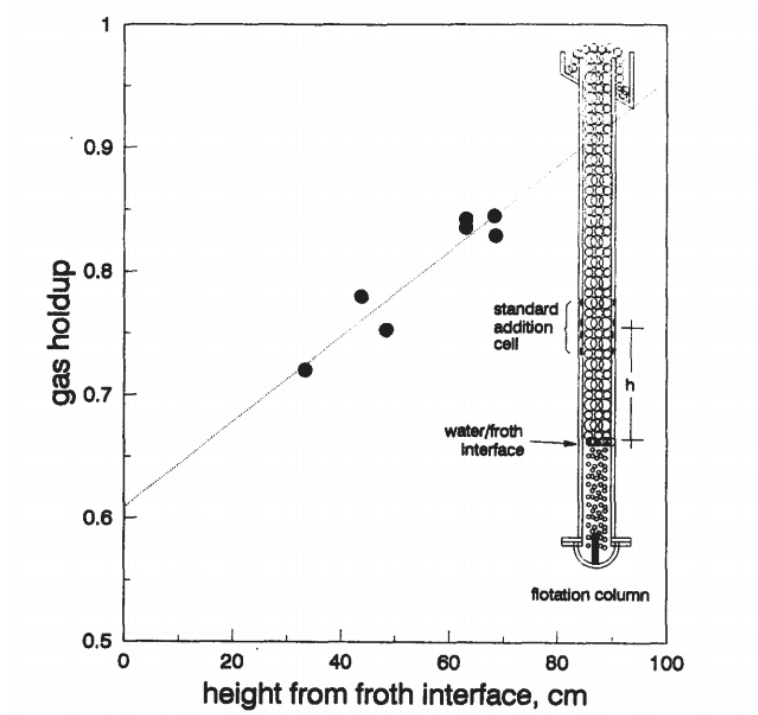


Figure 6.6: Study of Gas hold up in flotation froths. From Tavera et al. (1998)

Bibliography

- [1] S. Ata, N. Ahmed, and G.J. Jameson. “A study of bubble coalescence in flotation froths”. In: *International Journal of Mineral Processing* 72.14 (2003), pp. 255–266.
- [2] B.K. Gorain, M.C. Harris, J.-P. Franzidis, and E.V. Manlapig. “The effect of froth residence time of the kinetics of flotation”. In: *Minerals Engineering* 11 (1998), pp. 627–638.
- [3] C.Y. Mou and S.A. Adelman. “Transport properties of concentrated polymer solutions. Hydrodynamic mean field theory of the viscosity of a sphere suspension”. In: *Journal of Physical Chemistry* 69 (1978), 3146–3149.
- [4] S. J. Neethling and J. J. Cilliers. “Modelling flotation froths”. In: *International Journal of Mineral Processing* 72 (2003), pp. 267–287.
- [5] S. J. Neethling, H. T. Lee, and J. J. Cilliers. “Simple relationships for predicting the recovery of liquid from flowing foams and froths”. In: *Minerals Engineering* 16.11 (2003), pp. 1123–1130.
- [6] F.J. Tavera, C.O. Gomez, and J.A. Finch. “Estimation of gas hold-up in froth by electrical conductivity: Application of the standard addition method”. In: *Minerals Engineering* 11 (1998), pp. 941–947.
- [7] X. Zheng, J. P. Franzidis, and N. W. Johnson. “An evaluation of different models of water recovery in flotation”. In: *Minerals Engineering* 19.9 (2006), pp. 871–882.

Chapter 7

Conclusions

There has been considerable effort in recent years to approach operation of a flotation bank in a rational way to maximise the grade and recovery. Maldonado et al. (2011; 2012) used an isolated well-mixed cell kinetic model to compare the overall flotation recovery of two floatable minerals (A and B) with respect to different recovery profiles down the bank. They found that a balanced recovery profile maximises the separation ($R_A - R_B$) between two floatable minerals for a given bank target recovery of mineral A. A possible limitation of their analysis was that the relative floatability, S , was assumed to be constant along the bank and the pulp and froth zones were lumped. Using JKSimFloat, it was shown that regardless of variation in S and the magnitude of the froth zone recovery, the balanced recovery profile was still optimal.

The analysis of Maldonado et al., did not consider recovery of entrained mineral, E. JKSimFloat was used to solve for the case of entrained mineral. Mathematical analysis of the JKSimFloat water overflow rate model (Equation 7.1) led to the derivation of Equation 7.2.

$$Q_W = aQ_S^b \quad (7.1)$$

$$\frac{Q_{ENT,Bank}}{Q_{ENT,SingleCell}} = \frac{1}{n^{b-1}} \quad (7.2)$$

Equation 7.2 shows that for values of $b > 1$, entrainment recovery is minimised in a bank of cells operated with a balanced mass pull, compared to recovering all of the material from a single cell. Simulations conducted in JKSimFloat assuming $b > 1$ supported the mathematical analysis: the simulations found that a balanced mass

profile gives superior separation efficiency between a floatable and entrained mineral, and a balanced recovery profile gives a superior separation efficiency between two floatable minerals.

Equation 7.2 raises the question of what the range of b values would be for the flotation process, in general; i.e., if the value of b greater than one in every instance. If unity could be established as a lower limit for the value of b , it would imply that a balanced mass pull profile is a general solution for entrainment minimisation in a bank of flotation cells. Experimental data were collected in various flotation systems, using talc as a model hydrophobic solid, to investigate the range of b exponents in Equation 7.1. In each system tested, b was found to be greater than one. However, the inability to find a case in which $b < 1$ does not infer proof that b is *always* greater than one.

In an attempt to predict the value of b the gas hold-up in the froth and the value of α (as defined by Neethling et al. (2003)) were considered to form Equation 7.3:

$$Q_W = aQ_S^{\frac{\epsilon_{g,f}}{\alpha}} \quad (7.3)$$

This equation was used to fit the data obtained at the talc facility and showed reasonable predictive power for each cell in the rougher bank. It is appreciated that the fit used estimated rather than measured froth gas hold-up values but the values are realistic. While demonstrating an idea in one bank of cells is far from proving a general relationship, it may be worthwhile to fit Equation 7.3 to other data sets.

There is an implication if Equation 7.3 is proven to fit. A value of α less than 0.5 is typical for flotation systems (Neethling et al. 2003), suggesting that if the (fractional) gas hold-up in the froth is always greater than 0.5 the value of b would be greater than one. To be froth it is almost essential that the gas hold-up be greater than 0.5 (50 %), such that $b > 1$ may be a general solution. Equation 7.3 appears to merit further inspection.

Bibliography

- [1] M. Maldonado, R. Araya, and J.A. Finch. “Optimizing flotation bank performance by recovery profiling”. In: *Minerals Engineering* 24.8 (2011), pp. 939–943.
- [2] M. Maldonado, R. Araya, and J.A. Finch. “An overview of optimising strategies for flotation banks”. In: *Minerals* 2 (2012), pp. 258–271.
- [3] S. J. Neethling, H. T. Lee, and J. J. Cilliers. “Simple relationships for predicting the recovery of liquid from flowing foams and froths”. In: *Minerals Engineering* 16.11 (2003), pp. 1123–1130.

Appendix A

Conversion of Recovery Basis

It is possible to convert recovery from a bank feed basis to a cell feed basis (and vice-versa) for any cell (j) in a bank of n cells (Equation A.1).

$$R_{j,cellfeed} = \frac{R_{j,bankfeed}}{\prod_{j=1}^n (1 - R_{j,cellfeed})} \quad (\text{A.1})$$

Consider a balanced recovery profile, based on cell feed, such that the target recovery of the bank is 75 %. To divide this evenly among, n cells, a bank of cells is first considered (Figure A.1):

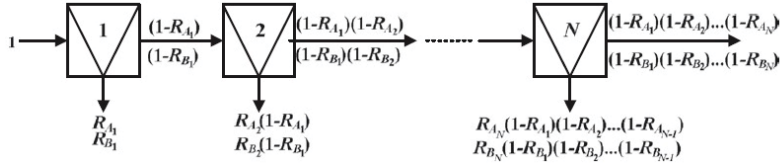


Figure A.1: Schematic of a bank of cells. From Maldonado et al. (2011)

For the n th cell in the sequence, assuming equal recoveries, the tailings can be rewritten as:

$$T_{A,n} = (1 - R_{A,i})^n \quad (\text{A.2})$$

To obtain the concentrate recovery, a mass balance around the bank can be taken to obtain:

$$R_{A,bank} = 1 - (1 - R_{A,i})^n \quad (\text{A.3})$$

For the target recovery (75 %) and 4 cells this yields a cell recovery of 29.3 %. It is possible to then use Equation A.1 to convert this profile from a cell feed basis to a bank feed basis. As such, Figure A.2 shows an identical bank strategy from two different viewpoints.

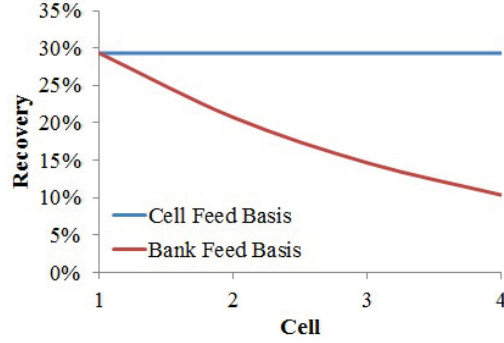


Figure A.2: Balanced recovery based on cell feed shown with respect to both bank and cell feed.

An extension of the analysis of Maldonado et al. (2011) is the ability to vary the value of S down the bank. From the returned mass pull of each mineral to the concentrate, the composition of the tailings stream can be calculated. From this composition and the floatability of each mineral, a weighted average floatability can be tabulated. A sample calculation of weighted average floatability for Cell 3 tailings is given:

$$P_{galena} = \frac{\sum f_{3,i} P_i}{\sum f_{3,i}} \quad (\text{A.4})$$

$$F_{Cell3,i} = F_{Bank,i} - C_{1,i} - C_{2,i} \quad (\text{A.5})$$

$$f_{3,i} = \frac{m_{i,galena}}{F_{cell3,i}} \quad (\text{A.6})$$

where P_i is the floatability of a given size class, i ; F is the mass flowrate in the feed of a given size class; C_i is the mass flowrate of concentrate from a cell of a given size class; $m_{i,galena}$ is the mass of galena in a given size class and $f_{3,i}$ is the assay of a mineral in a given size class.

Bibliography

- [1] M. Maldonado, R. Araya, and J.A. Finch. “Optimizing flotation bank performance by recovery profiling”. In: *Minerals Engineering* 24.8 (2011), pp. 939–943.

Appendix B

Raw Results

This appendix presents auxiliary data, reproducibility, and experimental checks for Chapters 4 and 5.

B.1 Experimental Check for the Miniature Column

The tailings flowrate was used to regulate the concentrate overflow rate in the miniature column. As a test of the experimental system the constant feed flowrate set using the distributor was plotted against the summation of the concentrate and tailings streams. Only two feed settings were used, however the calculated feed flowrates match these preselected feed settings as shown in Figure B.1.

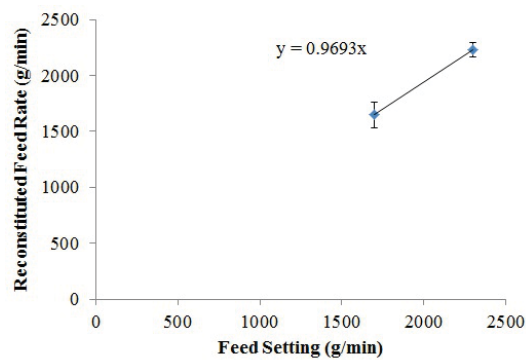


Figure B.1: Miniature column feed settings compared to the calculated feed.

B.2 Denver Cell DOE: Centre Point Repeats

The centre point repeats can be plotted as recovery–time curves to examine the reproducibility of each set of experiments (Figure B.2). The experiments for PPG 400 were conducted several months after those for 1–pentanol and sodium chloride, and it is expected that the difference in data is explainable by operator error.

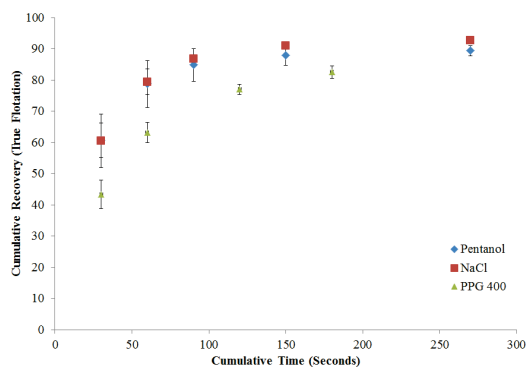


Figure B.2: Centre point repeats for the Denver cell design of experiment.

Appendix C

Discussion Calculations

The data used to fit the models used in Chapter 6 are presented in Table C.1.

Units	Parameter	Cell 1	Cell 2	Cell 3	Cell 4
<i>cm</i>	Cell Diameter	170.0	135.0	135.0	135.0
<i>cm</i> ²	A_cell	22698.0	14313.9	14313.9	14313.9
<i>cm</i>	Froth Height	25.4	20.3	15.2	15.2
<i>cm</i>	Froth Height above lip	10.0	5.0	5.0	5.0
<i>cm</i>	Sampling Depth (incl froth)	65.0	65.0	65.0	65.0
<i>cm</i> ³	Froth Volume	576529.4	290858.1	218143.6	218143.6
<i>cm</i>	Lip length	534.1	424.1	424.1	424.1
<i>mPas</i>	Viscosity	2.0	1.9	1.7	1.7
	% Solids	0.5	0.4	0.3	0.3
$\frac{m^3}{min}$	Air Rate 1	1.0	1.4	1.8	2.2
$\frac{m^3}{min}$	Air Rate 2	0.8	1.4	2.0	2.6
$\frac{m^3}{min}$	Air Rate 3	0.8	1.4	2.0	2.6
$\frac{m^3}{min}$	Air Rate 4	1.0	1.4	1.8	2.2
$\frac{cm}{s}$	Froth Velocity 1	1.3	3.0	3.0	3.6
$\frac{cm}{s}$	Froth Velocity 2	1.6	3.8	4.4	5.6
$\frac{cm}{s}$	Froth Velocity 3	1.6	3.6	5.0	2.6
$\frac{cm}{s}$	Froth Velocity 4	2.0	2.8	4.3	3.2
<i>mm</i>	<i>d</i> ₃₂ 1	0.9	1.0	1.1	1.0
<i>mm</i>	<i>d</i> ₃₂ 2	0.8	1.0	1.1	1.0
<i>mm</i>	<i>d</i> ₃₂ 3	0.9	1.0	1.1	1.1
<i>mm</i>	<i>d</i> ₃₂ 4	0.8	1.1	1.2	0.9

The values of α tabulated for this data is shown in Table C.2.

Table C.2: Tabulated values of alpha.

	Cell 1	Cell 2	Cell 3	Cell 4
Alpha 1	0.421	0.274	0.210	0.208
Alpha 2	0.623	0.348	0.280	0.275
Alpha 3	0.647	0.326	0.318	0.127
Alpha 4	0.631	0.256	0.302	0.183